nature reviews chemistry

https://doi.org/10.1038/s41570-023-00557-z

Review article

Designing electrolytes and interphases for high-energy lithium batteries

Hongli Wan , Jijian Xu & Chunsheng Wang

Abstract

High-energy and stable lithium-ion batteries are desired for next-generation electric devices and vehicles. To achieve their development, the formation of stable interfaces on high-capacity anodes and high-voltage cathodes is crucial. However, such interphases in certain commercialized Li-ion batteries are not stable. Due to internal stresses during operation, cracks are formed in the interphase and electrodes; the presence of such cracks allows for the formation of Li dendrites and new interphases, resulting in a decay of the energy capacity. In this Review, we highlight electrolyte design strategies to form LiF-rich interphases in different battery systems. In aqueous electrolytes, the hydrophobic LiF can extend the electrochemical stability window of aqueous electrolytes. In organic liquid electrolytes, the highly lithiophobic LiF can suppress Li dendrite formation and growth. Electrolyte design aimed at forming LiF-rich interphases has substantially advanced high-energy aqueous and non-aqueous Li-ion batteries. The electrolyte and interphase design principles discussed here are also applicable to solid-state batteries, as a strategy to achieve long cycle life under low stack pressure, as well as to construct other metal batteries.

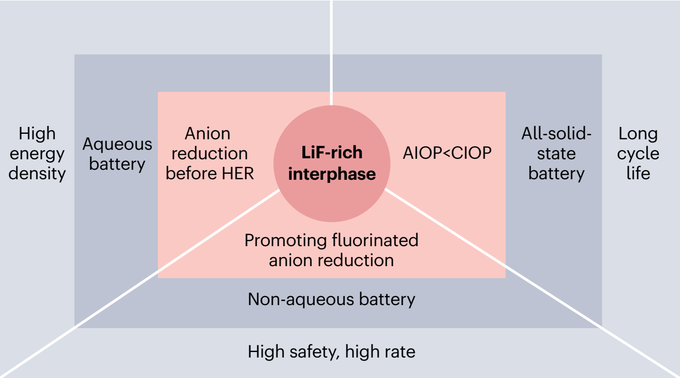

Sections

Department of Chemical and Biomolecular Engineering, University of Maryland, College Park, MD, USA.
e-mail: jijianxu@umd.edu; cswang@umd.edu

Introduction

Next-generation batteries, especially those for electric vehicles and aircraft, require high energy and power, long cycle life and high levels of safety[1–3]. However, the current state-of-the-art lithium-ion batteries using highly flammable organic liquid electrolytes have limited performance with a voltage window of less than 4.3 V[4]. To enhance the electrochemical performance of such batteries, rational electrolyte design and regulated interfacial chemistry are crucial for obtaining high-energy batteries that utilize high-capacity lithium metal or silicon anodes coupled with high-voltage cathodes.

Electrolytes function as a bridge for ion transport between the anode and cathode; they can be categorized as aqueous, non-aqueous liquid and solid-state electrolytes. The basic requirements for electrolytes are a high ionic conductivity and low electronic conductivity, a wide electrochemical stability window (ESW) or the ability to form a passive interphase, non-flammability and low cost. In 1859, the first rechargeable battery – Pb||PbO_2 (lead–acid) – was manufactured utilizing an aqueous electrolyte that relies on water as solvent[5]. Aqueous electrolytes offer intrinsic safety and fast-charging capability, and they are cost-effective; however, the ESWs of the electrolytes are constrained by the 1.23 V decomposition voltage of water[6], limiting the energy density of aqueous batteries. Through the formation of a LiF solid electrolyte interphase (SEI) via anion reduction at the anode and hydrophobic anion enrichment at the cathode, introduction of the 'water-in-salt' electrolytes substantially extended the ESW to 3.0–3.3V[7,8]. However, the cathodic stability potential (1.5–1.9 V) of water-in-salt electrolytes still limited the use of high-capacity graphite and Li metal anodes, thus still limiting the energy density of aqueous batteries. Non-aqueous, liquid carbonate electrolytes have a wide ESW of 4.2 V due to the formation of an organic–inorganic SEI at the anode and cathode electrolyte interphase (CEI) on the cathode. Use of the ethylene carbonate-based electrolytes enabled graphite anodes and $LiCoO_2$ cathodes to achieve a high Coulombic efficiency (>99.98%) and a lifetime of over 1000 cycles[9–11]. To further increase the cell's energy density, high-capacity Li and Si anodes and high-voltage cathodes must be utilized. However, the Li plating and stripping of the Li anode, and the lithiation–delithiation of Si anodes in carbonate electrolytes have Coulombic efficiencies below 90%, as the organic–inorganic SEIs are strongly bonded to Li and Si anodes, which leads to crack formation due to large changes in volume of the Si and Li anodes[12]. Additionally, high-voltage cathodes require the electrolytes to have a high oxidation stability by forming a robust CEI. Research has demonstrated that inorganic LiF-rich SEI and CEI can stabilize high-capacity Li and Si anodes and high-voltage $LiNi_{0.8}Mn_{0.1}Co_{0.1}O_2$ cathodes, which considerably enhanced the cycling stability of Li/$LiNi_{0.8}Mn_{0.1}Co_{0.1}O_2$ cells[13,14]. This is because the LiF-rich inorganic SEI–CEI has a high interface energy when in physical contact with a high-capacity anode and cathode, and it has a high redox stability, which lead to the LiF-rich inorganic SEI–CEI experiencing less stress and damage even if the high-capacity anodes and cathodes crack during discharging or charging processes. As the reduction of the organic solvent causes formation of organic–inorganic SEIs, whereas the reduction of the fluorinated anionic compound causes the formation of inorganic SEIs, the electrolyte design for high-voltage Li and Li-ion batteries has focused on promoting anion reduction but suppressing solvent reduction. The primary solvation shell of Li^+ has been proposed to represent the spheres of solvents that are closely coordinated to Li^+ (ref. 15). The species bound in this primary solvation shell would preferentially diffuse with the Li^+ ions to participate in interfacial reactions on the electrode surface. Since the interfacial reactions largely depend on the components in the Li^+ primary solvation shell[16], it is essential to increase the anion numbers in this shell, which can be achieved in, for example, high-concentration electrolytes, localized high-concentration electrolytes, weakly solvating electrolytes and softly solvating electrolytes[17–19]. However, decreasing the number of solvent molecules and increasing that of the anions in the solvation shell will come at the cost of ionic conductivity. Additionally, solvent reduction and SEI formation result in the consumption of both the solvent and Li from the cathode, causing cycle life and energy density to decrease. The correlation between the solvation structure of the electrolyte, SEI, CEI and ionic conductivity is still unknown; moreover, the electrolyte and Li inventory, and cycle life correlations also need to be investigated.

Solid-state electrolytes eliminated the use of solvents and attracted increasing attention due to their potentially high energy densities[20]. However, the narrow ESW of sulfide electrolytes and poor cathodic stability of halide electrolytes limit the application of a single-layer solid electrolyte in a lithium-metal battery with high-voltage cathodes[21]. This is because the formed SEI–CEI in the sulfide and halide electrolytes cannot suppress Li dendrite growth and support high-voltage cathodes, respectively. It is also very challenging to dope solid electrolytes with fluorine to form a LiF interphase. The fact that solid electrolytes have higher electronic conductivity than liquid electrolytes also carries with it additional challenges for Li nucleation inside solid electrolytes[22].

The performance of batteries is highly controlled by the properties of the interphase. In this Review, we mainly focus on how to form stable LiF-rich SEIs and CEIs that can withstand large volume changes of the high-capacity electrodes and high-voltage cathodes for high-energy batteries. Specifically, we will highlight strategies for electrolyte design to form LiF interphases and their impact on the batteries comprising different electrolytes, from aqueous electrolytes to organic liquid electrolytes, and, ultimately, solid electrolytes (Box 1). For organic liquid electrolytes, we correlate the solvation structure, interphase chemistry and interfacial energy when located against an anode and cathode with the said electrolytes' electrochemical performance. The LiF-rich inorganic interphases possess higher interface energies than organic interphases, and thus we discuss the strategies to promote anion reduction to form an inorganic interphase while suppressing the solvent reduction to minimize the formation of an organic interphase. As for the solid electrolytes, the correlation between the electro-chemo-mechanical properties of the solid electrolyte, SEI and lithium dendrite growth is discussed. To achieve high lithium dendrite suppression at a low stack pressure, interphase and interlayer design principles are discussed. The correlation between the electronic conductivity[22], ionic conductivity, lithiophobicity, porosity and the mechanical strength of interphases and interlayers are also discussed[23]. The latest knowledge of SEI–CEI composition and formation mechanisms, as well as future research needs, are discussed with the aim to push the scientific frontiers of the next-generation high-energy batteries.

Electrolytes for high-performance batteries

The electrolytes and the interphases (SEI and CEI) play the most critical role in battery performance. In a liquid electrolyte system, the interphase chemistries at electrode surfaces are dominated by the primary solvation structure of the Li^+ local environment, whereas bulk properties such as ionic conductivity, transference number, viscosity and wettability are mostly determined by the average composition of the bulk electrolyte. The transference number is defined as the fraction of ionic conductivity imparted by the lithium ion as opposed to its counterion, and it is the

Box 1

Designing the LiF-rich lithiophobic interfaces to solve the challenges at the electrolyte and electrode interface in different battery systems

Merits of LiF-rich lithiophobic solid electrolyte interphase (SEI) and cathode electrolyte interphase (CEI)

- LiF-rich SEI is critical to enabling the stability and reversibility of high-capacity anodes (Si and Li) undergoing large volume changes.
- LiF has a high interface energy (weak bonding) to Si, which enables the LiF SEI shell to remain cracking free when the Si core undergoes a large volume expansion/shrinking, preventing electrolyte penetration into the inner cracked Si to form new SEI, enabling pulverized Si to remain active.
- Highly lithiophobic LiF can promote Li diffusion along the Li–LiF SEI interface, but it can suppress Li penetration into LiF SEI due to high energy penalty.
- LiF SEI has a low area-specific resistance, enabling fast charging and operating at low temperatures.
- LiF-rich CEI with high anodic stability is key to stabilizing high-voltage and high-capacity cathodes.

Strategies to form LiF-rich lithiophobic SEI and CEI

- Promoting fluorinated anion reduction and suppressing solvent reduction.
- For aqueous electrolytes, use of ‘water-in-salt’ electrolytes enables anion reduction before the hydrogen evolution reaction. The secondary cations and eutectic effects can be used to stabilize H_2O and reduce hydrogen evolution reactions.
- For non-aqueous electrolytes, implementation of high-concentration, localized highly concentrated, weakly solvating and soft solvating strategies enhances anion reduction. By using these strategies in conjunction with solvents with a low reduction potential, such as tetrahydrofuran, solvent reduction can be inhibited.
- For solid electrolytes, a value for the applied interphase overpotential/critical interphase overpotential ratio below 1 is required, which can be realized by constructing porous and lithiophobic SEI or interlayer, and increasing the Li diffusivity of the Li metal anode.

Impacts

- Enabling the construction of batteries with high stability, high safety, high energy density and fast-charging capability.
- LiF SEI enables water-in-salt electrolytes to push the cathodic stability potential below 1.5 V with an electrochemical stability window of 3.3 V and beyond, making safe aqueous batteries more competitive.
- LiF SEI–CEI enables non-aqueous $Li/LiNi_{0.8}Mn_{0.1}O_2$ batteries to operate stably with high Coulombic efficiency under extreme conditions, such as fast charging and operation over a wide temperature range.
- LiF SEI or interlayer enables all-solid-state Li-metal batteries to operate at high capacity and high rate under low stack pressure.

transference number and conductivity that determine the flux of Li^+ (refs. 24,25). In a solid electrolyte system, lithium dendrite growth is highly correlated to the properties of the SEI, including lithiophobicity, mechanical characteristics, and electronic and ionic conductivity. Therefore, understanding the interfacial reactions and properties of the formed SEI–CEI is essential. Taking the fast-charging property in liquid electrolytes as an example, this property relies on the solvated Li^+ transportation in the bulk electrolyte and also on the desolvation process close to the interphases and subsequent diffusion of naked Li^+ across the SEI–CEI. In this section, we will mainly discuss the key scientific challenges related to electrolytes for liquid and all-solid-state batteries (Fig. 1a).

Electrochemical stability window

Batteries utilizing high-capacity Li and Si anodes, high-voltage and high-capacity cathodes, or a combination of these, are effective strategies for pursuing higher energy densities. Replacing the conventional graphite anode (specific capacity: 372 mAh g^{-1}) with Si (3,579 mAh g^{-1}) or Li (3,860 mAh g^{-1}) anodes can increase the theoretical electrode-level energy density from 468 Wh kg^{-1} (graphite||LMO_2; L = Li, M = Ni, Co or Mn) to 618 Wh kg^{-1} (Si||LMO_2) and 701 Wh kg^{-1} (Li||LMO_2) (blue line in Fig. 1b). From these data, it can be deduced that high-capacity and high-voltage cathodes are required to match the Li (red line) or Si (pink line) anodes to achieve greater energy density. Increasing the upper cut-off voltage is the most straightforward method for increasing the specific capacity of layered cathodes (LMO_2). For example, by changing the upper cut-off voltages from 4.3 V to 4.6 V, the capacity of $LiCoO_2$ increases from 170 mAh g^{-1} to 220 mAh g^{-1} (ref. 26). Nevertheless, considerable cathode surface reconstruction and transition metal dissolution are initiated if the CEI is not stable when charging above 4.4 V. A robust CEI is required to suppress side reactions during high-voltage operations. It is important to note that operation voltages above 4.3 V exceed the oxidation stability of conventional carbonate-based electrolytes. From this perspective, the ESW of the electrolyte should be as wide as possible to support high-voltage cells.

Electrolyte solvation structure, SEI and CEI

It is widely acknowledged that SEI–CEI formation provides kinetic protection and thus extends the ESW of electrolytes[1,27]. Among various strategies, tailoring the SEI–CEI layers via electrolyte design is the most powerful and effective. An ever-growing number of lithium salts, solvents and additives have been developed for advanced electrolytes with considerable promise. In addition to using the lowest unoccupied molecular orbital and highest occupied molecular orbital energy as a qualitative assessment of possible redox stability, the solvation

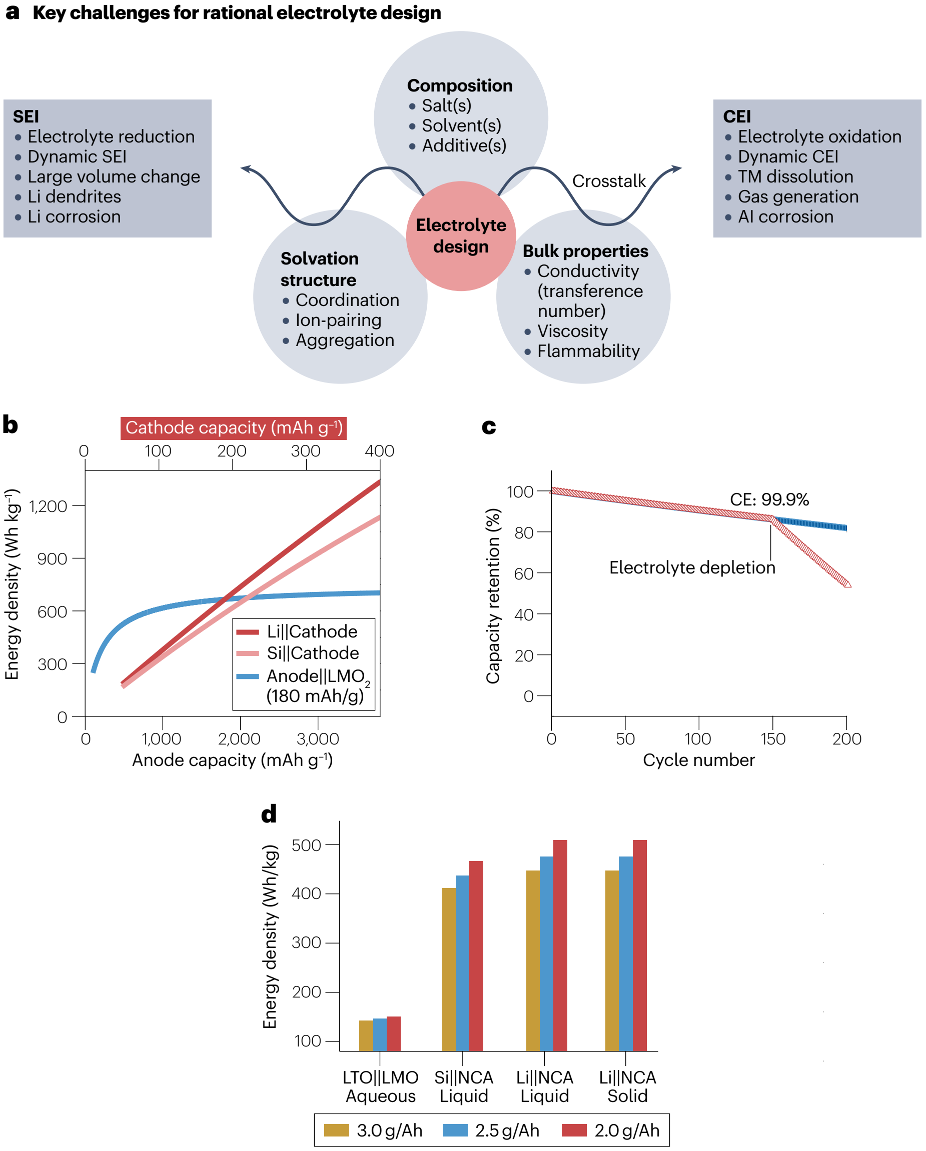

Fig. 1 | Key scientific challenges when designing electrolytes. a, A range of factors that have to be considered for electrolyte design, including electrolyte composition, bulk properties and the solvation structure, in order to address key scientific problems associated with solid electrolyte interphase (SEI)–cathode electrolyte interphase (CEI) interphases. **b**, The projected energy density as a function of the anode capacity (blue curve, the LMO$_2$ capacity is set to 180 mAh g^{-1}) and cathode capacity (red curve for a Li||Cathode cell and pink curve for a Si||Cathode cell). **c**, Capacity retention in a theoretical cell with a Coulombic efficiency (CE) of 99.9% (blue curve) and a lean electrolyte (red curve) with rapidly decreasing retention capability at the point of electrolyte depletion. **d**, Energy density data across different commonly used systems showing that a greater density is observed in liquid and solid-state energy storage devices than in aqueous systems. The theoretical energy density is determined by the cathode and anode chemistry, in a situation in which the amount of electrolyte (2.0; 2.5; 3.0 g Ah^{-1}) affects the practical energy density in cells. LMO, LiMn$_2$O$_4$; LMO$_2$, L = Li, M = Ni, Co or Mn; LTO, Li$_4$Ti$_5$O$_{12}$; NCA, LiNi$_{0.8}$Co$_{0.15}$Al$_{0.05}$O$_2$; TM, transition metal.

structure of the electrolyte should also be considered[28,29]. There is a growing appreciation for the role of the solvation structure and SEI–CEI interphase towards electrode performance, but a relationship between them is still lacking due to the complex and dynamic nature of SEI–CEI composition. Benefiting from the development of cryo-scanning transmission electron microscopy, the SEI in 1 M LiPF$_6$ ethyl carbonate/diethyl carbonate was observed with a large swelling ratio, indicating that 50% of the SEI volume is composed of the liquid electrolyte[30]. In sharp contrast to this observation, inorganic-rich SEI in 4 M lithium bis(fluorosulfonyl)imide (LiFSI) – dimethoxyethane exhibited a smaller swelling ratio (10.9 nm versus 8.8 nm). The Coulombic efficiency results further suggest that a decreased swelling ratio in inorganic-rich SEI correlates to an increased Coulombic efficiency. With emerging advanced characterization techniques and machine learning, we might be able to establish predictive models to analyse the effect of the solvation structure on the formation and evolution of SEI–CEI interphases[31–33].

Electrolyte depletion

The use of high-capacity Li and Si anodes requires excess electrolytes, in consideration of the consumption of the electrolyte caused by side reactions. Most of the previously reported electrochemical performances are assessed by coin cells; the presence of flooded electrolytes in the cell may contribute to improved cycling performance due to a reduced reliance on electrolytes in the cell, and it also effectively improves high-rate performance. The effect of the Coulombic efficiency on full-cell capacity-retention assumes that other factors do not influence cycling performance (Fig. 1c; blue line). With a Coulombic efficiency of 99.9%, a full cell retains 81% of its initial capacity after 200 cycles. Understandably, the capacity of the full battery will drop faster when the electrolyte is depleted (Fig. 1c; pink line). It was found that reducing the electrolyte amount from 25 g Ah^{-1} to 3 g Ah^{-1} drastically reduced the cycle life of 250 μm Li||LiNi$_{0.8}$Mn$_{0.1}$Co$_{0.1}$O$_2$ (3.8 mAh cm^{-2}) from 60 cycles to ten cycles[34]. The amount of electrolyte also plays a vital role in determining energy density. By considering the electrolyte amount, the specific energy densities of Si||LiNi$_{0.8}$Co$_{0.15}$Al$_{0.05}$O$_2$ full cells are 467 (2.0 g Ah^{-1}), 438 (2.5 g Ah^{-1}) and 412 (3.0 g Ah^{-1}) Wh kg^{-1}, and the specific energy densities of Li||LiNi$_{0.8}$Co$_{0.15}$Al$_{0.05}$O$_2$ full cells are 509 (2.0 g Ah^{-1}), 476 (2.5 g Ah^{-1}) and 447 (3.0 g Ah^{-1}) Wh kg^{-1} (Fig. 1d). Solid electrolytes have the potential to decrease the amount of electrolyte to less than 2.0 g Ah^{-1} while granting a higher energy density. Other inactive materials including separators, current collectors and package materials need to be considered at cell level. From the early 2020s, different scientific journals initiated an experimental checklist in an effort to standardize battery performance purporting and to try to minimize experimental data misinterpretations[35].

Practical considerations for electrolytes

Practical requirements, including cost, operating in a wide range of temperatures and lifespan, need to be taken into account when designing an electrolyte. For example, the cost is always the primary factor in commercializing a new lithium salt, solvent or additive. In the conventional LiPF$_6$ and carbonate-based electrolytes, LiPF$_6$ is the main cost driver, accounting for 40–60% of the raw material cost[36]. The last few decades have witnessed a continued trend towards lower LiPF$_6$ prices along with the expansion of the electrolyte market. This means that when electrolyte components are mass-produced, the cost can be reduced due to scaling effects. It is reasonable to remain open to newly developed electrolyte components while carefully evaluating their abundance and availability, as well as the security of raw materials and the recycling prospects.

Aqueous electrolytes are, in theory, very low-cost, yet problems primarily associated with the longstanding 'cathodic limit' have severely limited energy densities (<150 Wh kg^{-1}). Solid electrolytes have received much attention due to the abundance of their constituent parts, but they face manufacturing difficulties, as the thickness of the solid electrolyte is difficult to reduce to less than 100 µm without sacrificing ionic conductivity. The average price for non-aqueous Li-ion batteries was US $135 kWh^{-1} in 2022, which is higher than the price of aqueous lead–acid batteries, at a cost of US $65 kWh^{-1}. Meanwhile, all-solid-state batteries are still in their early stages of commercialization. Overall, a commercially viable cost target at the battery pack-level is generally acknowledged to be US $75–80 kWh^{-1}. Beyond basic cost considerations, advanced electrolytes should be capable of operating over a wide range of temperatures. Many areas experience winter temperatures below freezing and battery performance at temperatures of −10 °C or −20 °C is an important operational factor. Unfortunately, conventional carbonate-based liquid electrolytes freeze when the temperature decreases to −20 °C, resulting in unsatisfactory battery performance[37]. High temperature stability is another challenge for electrolytes, in conditions in which, for example, the widely used LiPF$_6$ electrolyte is highly vulnerable to hydrolysis and decomposes to form corrosive HF at the temperature of 60 °C[38]. Furthermore, the organic interphase can dissolve into electrolytes at high temperature, and, even worse, transition metal dissolution of LMO$_2$ cathodes becomes more severe at high temperatures[39]. High-temperature operation requires electrolytes with high thermal stability and thermally stable interphases with low solubility. Ideally, SEIs and CEIs should not dissolve upon charging and discharging, and they should protect the electrodes[40]. Without an effective SEI passivation, the electrolyte and Li will be consumed continuously as the device ages due to Li corrosion through a galvanic process in which Li and Cu serve as anode and cathode, respectively[41]. Likewise, the lifetime of Si-anode batteries is still only 20–30 months, far below the automotive applications requirement of ~120 months[42]. The key challenge regarding aging is that evaluation and diagnosis are very time-consuming and smarter strategies are desired to accelerate aging processes to study the systems over shorter timespans to ultimately understand how to extend their lifetimes, as well as expand the temperature range over which batteries efficiently operate.

Electrolyte design principles

In this section, we establish universal electrolyte design principles to achieve high-performance lithium-metal and lithium-ion batteries by preferentially decomposing anions instead of the solvent to form inorganic-rich interphases (Fig. 2a). The invention of the 21 molality water-in-salt hailed the beginning of the 'solvent-in-salt' regime[7], which inspired the use of highly concentrated non-aqueous electrolytes with almost no free solvent[19]. Solid electrolytes with no solvent can be viewed as the most extreme case of this idea (Fig. 2b), but they also suffer from the difficulty of forming a LiF-rich interphase. Importantly, the interfacial chemistries among aqueous, non-aqueous and solid electrolytes are in fact highly related.

Aqueous electrolytes

Aqueous Li-ion batteries are typically limited to low voltages (<1.5 V) due to the narrow ESW of water (1.23 V) and the lack of protective interphases. Expanding the ESW of aqueous electrolytes is highly dependent on the formation of a passivating interphase at the anode and hydrophobic anion absorption on the cathode. The invention of water-in-salt electrolytes with an anion-containing Li$^+$ primary solvation structure makes anion-derived LiF-rich SEIs possible, which has afforded a considerable enhancement of the aqueous ESW to 3.0 V[7] (Fig. 2b). Here, water-in-salt is defined as the region in which the salt exceeds the solvent in terms of both weight and volume. Following the same pattern, extensive efforts have been devoted to aqueous electrolytes by further increasing the salt concentration and adding organic solvents[43]. However, the use of highly concentrated lithium salts and organic solvents deviates from the aim of reducing cost and enhancing safety when developing aqueous electrolytes. It should also be noted that the cathode limit only extends from 1.90 V to 1.75 V, even when the salt concentration increases from a molality of 21 to a molality of 63 (ref. 44). Aside from the concentration, knowledge of other decisive factors that can be used for widening the ESW is crucial.

One decisive factor is the primary Li$^+$ solvation structure and the derived interphases. A 4.5 molality LiTFSI-KOH-CO(NH$_2$)$_2$-H$_2$O electrolyte has been developed, which enabled 2.5 mAh cm^{-2} LiMn$_2$O$_4$||Li$_4$Ti$_5$O$_{12}$ full cells to achieve an average Coulombic efficiency of ~99.9% and superior cycling stability[8]. The high performance is attributed to the reduced number of H$_2$O molecules in the Li$^+$ solvation shell and the formation of LiF and a polymer bilayer SEI. Likewise, CO$_2$ was introduced as an interphase-forming-additive in 5 molality LiTFSI-H$_2$O electrolyte to form Li$_2$CO$_3$-rich SEI, resulting in a similar cycling performance as that of 21 molality LiTFSI water-in-salt electrolyte[45]. As for the various hybrid aqueous and non-aqueous electrolytes, the common features are the presence of anions in the Li$^+$ primary solvation sheath and the onset of the anion reduction before the occurrence of the hydrogen evolution reaction of water[46–48]. In a broader context, these studies have deepened our understanding of the complex solvation structures generated by various electrolyte components and how to manipulate and tune their interfacial chemistry.

Non-aqueous electrolytes

When the concept of solvent-in-salt is applied to organic electrolytes, there are many possible variants, such as 'highly concentrated electrolyte', 'localized highly concentrated electrolyte' and 'weakly

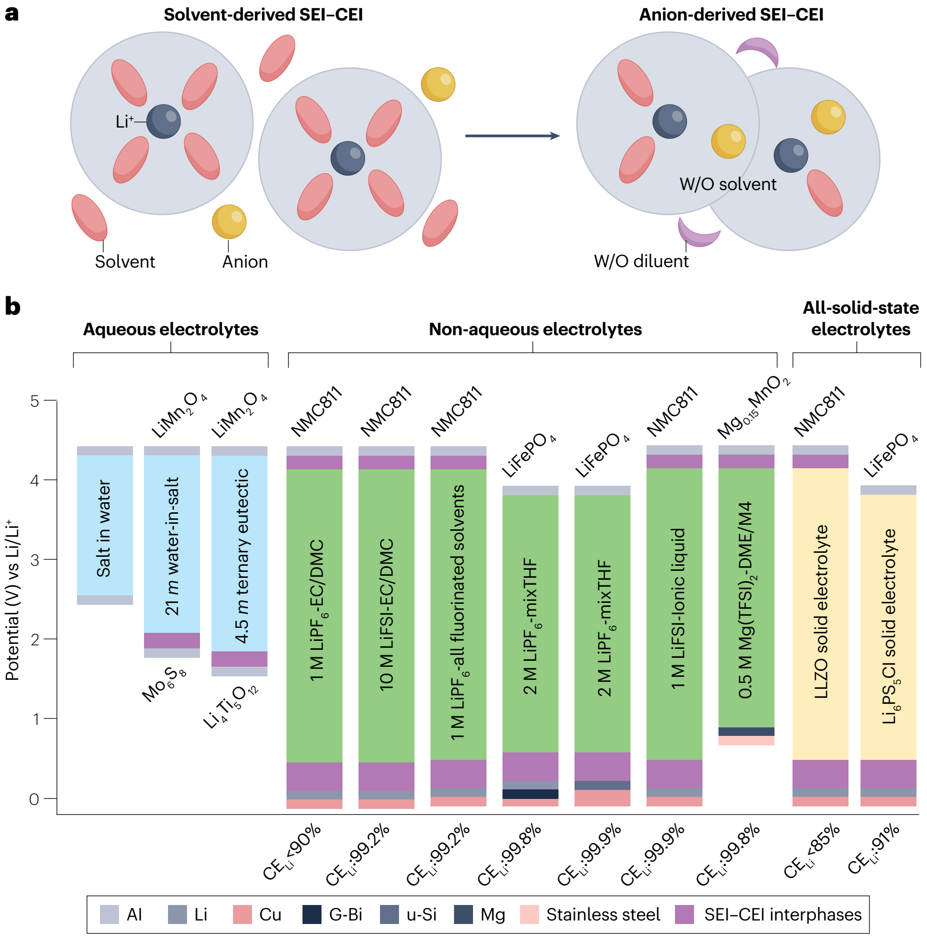

Fig. 2 | Illustration of the universal electrolyte design principles. a, Comparison of solvation structures. Left: solvation structure of 1 M carbonate-based electrolyte with interfacial reactions dominated by solvent decomposition resulting in an organic-rich solid electrolyte interphase–cathode electrolyte interphase (SEI–CEI). Right: solvation structure of advanced electrolytes in which anions also compose the primary solvation shell, enabling anion decomposition and the formation of inorganic-rich SEI–CEI. **b**, Typical electrolytes, from aqueous to non-aqueous and solid electrolytes, with varying Coulombic efficiencies (CE) and electrochemical stability windows (ESWs) as seen by the potentials versus Li/Li$^+$. CE$_{Li}$, Coulombic efficiency of Li; DMC, dimethyl carbonate; DME, 1,2-dimethoxyethane; EC, ethylene carbonate; G-Bi, bismuth graphite blend; LLZO, $Li_7La_3Zr_2O_{12}$; M4, 1-methoxy-2-propylamine; NMC811, $LiNi_{0.8}Mn_{0.1}Co_{0.1}O_2$; FSI, bis(fluorosulfonyl) imide; THF, tetrahydrofuran; mixTHF, mixture of THF and 2-methyltetrahydrofuran; TFSI, bis(trifluoromethylsulfonyl)amine; u-Si, microsized Si; W/O, without.

solvating electrolyte'. Non-aqueous highly concentrated electrolytes generally have a salt concentration greater than 3 M, depending on the solvent's capability to dissolve salts[49,50]. Therefore, tentative suggestions have been made to classify electrolytes by focusing on whether an anion is involved in the primary solvation sheath, rather than by defining a specific concentration value[43]. The anion in the primary active cation solvation shell is used to promote anion reduction to form inorganic LiF-rich interphases; which enables high-capacity or/and high-voltage electrodes to achieve a long cycle life due to decreased bonding between the LiF interface and these electrodes. The so-called localized highly concentrated electrolyte is a clever improvement on highly concentrated electrolytes, which consists of the introduction of non-solvating diluents as a way to change the salt concentration to 1 M or lower, while maintaining the merits of a high-concentration electrolyte. Another promising approach is to directly reduce the solubilizing capability of the solvents so that the anion participates in the solvation sheath at low concentrations – weakly solvating electrolyte approach[51]. Soft solvating electrolytes, which minimize the Li$^+$ solvent binding energy while still dissociating the lithium salt, have also been developed; they achieve exceptional performance under extreme operating conditions (±60 °C)[17]. These strategies lead to the generation of electrolytes with prevailing ion pairs and aggregates, resulting in anion-dominated interphases but sacrificing ionic conductivity. Forming a LiF-rich interphase while still maintaining a high ionic conductivity is critical for the devise of next-generation organic electrolytes.

Advances in SEI chemistry for high-capacity anodes. The adoption of ethylene carbonate on graphite surfaces to form flexible organic–inorganic SEI is key to the commercialization of graphite||$LiCoO_2$ Li-ion batteries[9]. However, organic–inorganic SEIs formed in carbonate electrolytes are not robust enough to accommodate the volume expansion of high-capacity Li and Si anodes. To avoid the SEI fracturing, an inorganic-rich interface is designed to bond weakly with the anode surface. Due to the lithiophobicity of the obtained SEI, and the resulting weak bonding to Li, it can effectively accommodate the volume change during Li plating and stripping, and it promotes Li lateral diffusion along the Li side of the SEI but suppresses Li penetration into the lithiophobic SEI. Since inorganic species including LiF, Li_2O and Li_2CO_3 possess a high Young's modulus and high lithiophobicity, they can effectively suppress Li dendrite penetration into the SEI[13]. The nature of the SEI is critical for the stabilization of high-capacity anodes (Si and Li)[22,52–62].

Si anodes undergo a large volume change during lithiation and delithiation, and, as a consequence, the SEI is more likely to crack, delaminate and show more dynamic evolution than the interface on graphite surfaces. The large volume change and polarization of Si will break the organic–inorganic SEI, resulting in electrolyte penetration into the cracked Si and the continuous formation of new SEIs. Solid-state NMR revealed that the products of ethylene carbonate decomposition are dominated by oligomeric species, which are easily cracked, leading to the exposure of the reductive Li_xSi_y surface to the electrolyte and to the continuous depletion of the electrolyte, resulting in fading capacity[63]. The addition of fluoroethylene carbonate to conventional electrolytes has been reported to result in the generation of a LiF-containing SEI, a process initiated by fluoroethylene carbonate reduction and radical polymerization[64]. Nevertheless, polymer-rich SEIs can still not fully withstand the large stresses caused by the large volume change of Si during lithiation, resulting in unsatisfactory performance[65]. Following the strategy of building a highly elastic SEI that bonds strongly to the Si surface, the elastic binders improved the cycling performance of the 1–3 μm Si particles[66–68], but the cycling Coulombic efficiency was still unsatisfactorily low for commercialization (Coulombic efficiency<99.7%; cycle life<50). A different strategy is to form the SEI characterized by weak bonding interactions with the Si anodes and high mechanical strength, allowing the lithiated alloys to undergo plastic deformation inside the SEI without damaging it. LiF has been selected as a suitable SEI candidate because it possesses the highest interfacial energy with Li_xSi_y. In addition, a LiF inorganic interphase with a high ionic:electronic conductivity ratio reduces the thickness of the SEI and area-specific resistance, increasing the initial Coulombic efficiency of the first cycle. LiF-rich SEIs with high interfacial energy when in physical contact with high-capacity anodes enable micro-sized Si and Li anodes to achieve long cycle life[69]. Specifically, LiF SEIs are preferentially formed from $LiPF_6$ decomposition starting at high potentials by designing electrolytes with a high degree of $LiPF_6$ salt aggregation and the lowest solvent reduction potential.

The practical application of Li metal is mainly hampered by the notorious Li dendrites, which lead to continuous electrolyte depletion, low Coulombic efficiency, formation of 'dead Li' and, ultimately, battery failure. Considering the critical role of SEIs in suppressing Li dendrites, a comparative analysis of the SEI composition will also be discussed. A combination of interface energy and Young's modulus of the SEI has been adopted as a criterion to assess Li-dendrite suppression capability. As listed in Table 1, the LiF component with the highest interface energy and Young's modulus can effectively suppress Li penetration into the SEI due to the high-energy penalty. In addition, LiF has a low area-specific resistance due to the high ionic:electronic conductivity ratio. To form a LiF-rich SEI, research has largely focused on fluorinated solvents and additives[70–72]; however, organic components are inevitably generated through solvent reduction (Fig. 3a,b). The reduction of electrolytes can be further tuned by the solvent-in-salt strategy — elevating the reduction potential of anions via aggregation, and choosing solvents that undergo reduction at a lower voltage, so that salt-derived SEIs are preferentially formed (Fig. 3c,d). For example, the LiF-rich SEI can be successfully formed via LiFSI salt reduction by simply increasing the LiFSI concentration in carbonate electrolytes due to the formation of aggregated anions in the solvation shell of Li^+ (refs. 73–80). Despite all these efforts, Li Coulombic efficiencies are still around 99.5%[12]. Achieving a Coulombic efficiency higher than 99.9% may require a solvent-free electrolyte to completely avoid solvent reduction[81].

LiH is characterized by a higher ionic conductivity than LiF[82,83] — $\sigma(LiH) = 10^{-10}$ S cm^{-1} versus $\sigma(LiF) = 10^{-31}$ S cm^{-1}. However, the band gap of LiH is much smaller than that of LiF (Table 1), which means that LiH is not as stable as LiF at high potentials. The possible formation of LiH in batteries was once overlooked due to its strong reductive properties. The first attempt to explore the possible LiH formation induced by unavoidable water contamination was performed using surface-sensitive Fourier-transform infrared spectroscopy in 1999 (ref. 84). Although LiH was not detected by titration gas chromatography[85], the existence of LiH[86] was identified through cryo-scanning transmission electron microscopy, synchrotron-based X-ray diffraction and mass spectrometry titration techniques[86–88]. It was revealed that lithium can react with H_2 — generated by hydrogen evolution side reactions — to form LiH[89]. Although the influence of LiH on the SEI has been discussed in several papers, it remains unclear whether LiH increases or decreases the stability of Li metal anodes, as different experiments have pointed to different conclusions; some demonstrated the positive role of LiH in promoting Li-ion diffusion[90], whereas others state that the existence of LiH is detrimental to SEI stability and leads to the formation of dead Li[89,91]. From the perspective of interfacial regulation, the combination of mechanically stable LiF and ionically conductive LiH as building species for the SEI may afford the construction of ideal interfaces characterized by fast Li^+ diffusion kinetics and the ability to inhibit Li dendrite growth.

Advances in CEI chemistry for high-voltage cathodes. Improvements in cathode technology need to be made to match the energy density of anodes and obtain the highest energy storage out of the battery (Fig. 1b). The role of the CEI was once overlooked because it was thought that there was no thermodynamic driving force for electrolyte oxidation in commercial batteries operating at voltages below 4.3 V[92–94]. Under high-voltage operation (>4.3 V), the decomposition of ethylene carbonate-based conventional electrolytes was found to be dominated by ethylene carbonate open-ring reactions accompanied by obvious oxygen loss[95–97]. Introducing a CEI-forming additive containing boron[98,99], nitrogen[100], fluorine[101], phosphorus[102,103], sulfur[104] or a combination of these elements in the conventional electrolyte can effectively enhance its oxidation stability[105,106]. However, these

Table 1 | Comparison of physical properties and calculated parameters of different interphase components that listed in Table 1

Composition	Crystal structure	E_g (eV)	σ_{Li} (s cm^{-1})	Young's modulus (GPa)	Interfacial energy (meV Å^{-2})
LiF	Cubic, $a = 4.08$ Å	8.65	10^{-31}	70	73.28
LiCl	Cubic, $a = 5.15$ Å	6.31	10^{-14}	32	37.55
LiBr	Cubic, $a = 5.51$ Å	5.03	10^{-10}	21	–
LiI	Cubic, $a = 6.03$ Å	4.28	10^{-7}	21	–
LiH	Cubic, $a = 4.00$ Å	2.98	10^{-10}	36	–
LiOH	Tetragonal, $a = 3.59$ Å	4.01	10^{-11}	10	–
Li_2O	Cubic, $a = 4.66$ Å	4.90	10^{-10}	78	38.70
Li_2S	Cubic, $a = 5.72$ Å	3.49	10^{-13}	40	19.01
Li_2CO_3	Monoclinic, $a = 8.52$ Å	5.06	10^{-10}	63	59.22
Li_3N	Hexagonal, $a = 3.65$ Å	0.98	10^{-3}	74	32.13
Li_3P	Hexagonal, $a = 4.24$ Å	0.88	10^{-2}	30	45.64

To form a solid solution with LiF, the same cubic structure is the first requirement, which thereafter can lead to other crystal structures. Hence, lattice parameters for the other crystal structures have been omitted and only the 'parent' cubic phase parameter is shown. E_g, Energy gap; σ_{Li}, Li ionic conductivity.

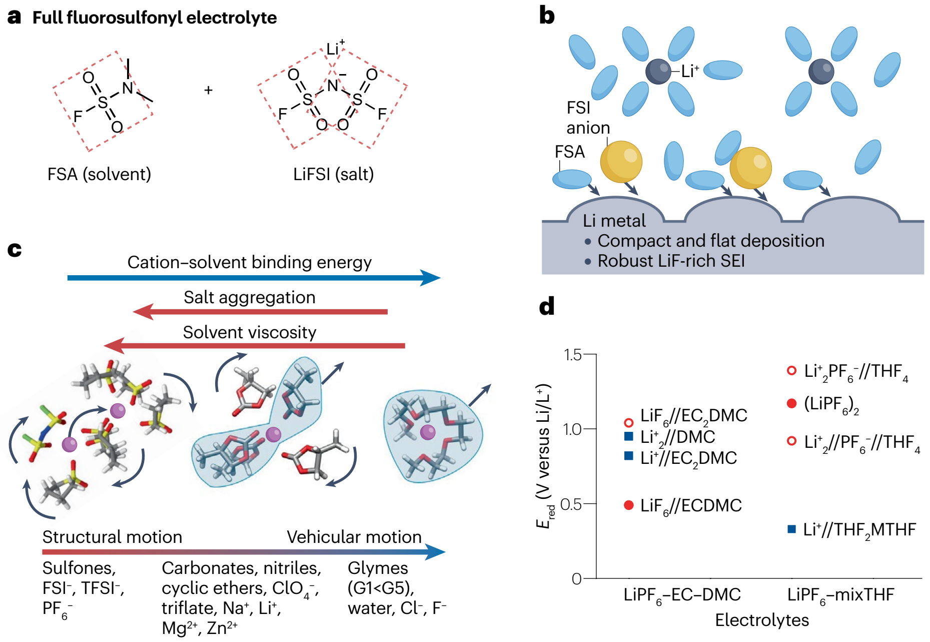

Fig. 3 | Design strategies for the LiF-rich solid electrolyte interphase (SEI). **a**, Chemical structures of N,N-dimethylsulfamoyl fluoride (FSA) solvent and lithium bis(fluorosulfonyl)imide (LiFSI) salt. The red dashed boxes outline the same fluorosulfonyl groups. **b**, Illustration of interfacial reactions in the electrolyte, where the fluorosulfonyl groups in the FSA and FSI contribute to forming an LiF-rich SEI[72]. **c**, Summary of the parameters that determine the electrolyte properties[43]. In vehicular motions, the solvation sheath travels with the solvated ion, whereas the ion hops in structural motions. Weaker ion-solvent binding, higher salt aggregation and higher solvent viscosity make the transport motion more structural, favouring the formation of an inorganic-rich SEI. G1, monoglyme; G5, pentaglyme. **d**, Results of density functional theory calculations of the reduction potentials of various electrolyte components, indicating the preferential reduction of anions over solvents[69]. Red symbols represent anion reduction and blue symbols represent solvent reduction. Squares denote fully dissociated Li^+ species, whereas circles denote species undergoing ionic aggregation. DMC, dimethyl carbonate; EC, ethylene carbonate; MTHF, 2-methyltetrahydrofuran; TFSI, bis(trifluoromethylsulfonyl) amine; THF, tetrahydrofuran; mixTHF, mixture of THF and MTHF. Parts **a** and **b** adapted from ref. 72, CC BY 3.0 ; part **c** adapted with permission from ref. 43, Elsevier; part **d** adapted from ref. 69, Springer Nature Limited.

additives will gradually be consumed through the interfacial reactions, thus eventually causing a deterioration of the cycling stability of lithium-ion cells. In addition, most CEIs formed by the oxidation of solvents mainly comprise organic components, which can be oxidized at a higher voltage and cannot fully withstand the large volume change taking place during lithiation and delithiation[107,108]. Similarly to the case of anodes, inorganic-rich CEIs with weak bonds to the cathodes are crucial for inhibiting cathode structural damage and electrolyte penetration, thus enhancing the cathode cycle life at a high voltage. The challenge is to form inorganic-rich CEIs, especially LiF-rich CEIs, because LiF has the largest band gap and is the most thermodynamically stable. Fluorinated solvents have been reported to contribute to the formation of LiF in CEI[73,109,110]. For instance, the CEIs derived from a 1 molality LiFSI and N,N-dimethyltrifluoromethane-sulfonamide electrolyte mainly consist of LiF-like inorganic species, enabling stable cycling of $LiNi_{0.8}Mn_{0.1}Co_{0.1}O_2$ at the high voltage of 4.7 V[111]. Essentially, use of solvent-in-salt electrolytes with an abundance of aggregations leads to more LiF inorganic components and less organic components in CEIs[19,50,112–115]. A remarkable self-healing ability of a LiF-dominated CEI was seen in situ by visualization of the CEI formation in an $LiPF_6$ and propylene carbonate electrolyte using environmental transmission electron microscopy[14]. The results of density functional theory calculations suggest that FSI^- anions and fluorinated fragments derived from the decomposition of FSI^- anions may contribute to LiF formation considering the nonviability of the direct oxidation of anions[116,117]. As a step out of the labyrinth of oxidation, a dense LiF-rich CEI was formed by electrolyte reduction at 1.7 V[118].

Based on the results reported in the literature so far, both oxidation and reduction approaches can afford the formation on LiF-rich CEI. The fundamental criteria for electrolyte design are consistent with those already mentioned: promoting anion decomposition (via oxidation or reduction) and suppressing solvent decomposition. Overall, the ideal electrolytes can not only suppress Li dendrite growth by forming self-limiting, compact SEIs, but they also stabilize the CEI of high-voltage cathodes, thus improving the electrochemical performance of high-energy batteries.

Solid electrolytes

Lithium dendrite growth is the main challenge restricting the practical application of all-solid-state Li-metal batteries (ASSLBs). The growth of lithium dendrites is affected by the electro-chemo-mechanical properties of both solid electrolytes and SEIs. Therefore, designing stable electrolytes and interphases with high lithium dendrite suppression capabilities is crucial for ASSLBs.

Lithium dendrite formation and growth. In the battery community, there is still no consensus regarding the growth mechanisms of lithium dendrites in ASSLBs. The chemical, electrochemical and mechanical properties of the solid electrolyte and SEI will impact lithium dendrite formation, as well as lithium dendrite growth at the solid electrolyte–Li interface and inside the solid electrolyte. Studies evaluating the chemical and electrochemical stability of solid electrolytes propose that Li metal can nucleate inside solid electrolytes due to the electronic conduction of the said electrolytes[22,119,120]. Research considering the mechanical properties of solid electrolytes propose that defects (cracks, flaws and grain boundaries) in solid electrolytes are the main reason for lithium dendrite formation and growth. However, even a single-crystalline $Li_6La_3ZrTaO_{12}$ solid electrolyte cannot prevent lithium dendrite growth[121]. Therefore, a third lithium dendrite growth mechanism, that is, the electro-chemo-mechanical model, was proposed[53,122], which considers the chemical, electrochemical and mechanical properties of the solid electrolyte. Herein, we limit our discussion to the third mechanism. For example, it is possible that the solid electrolyte is not stable during Li plating at a negative potential, leading to the formation of an SEI where the Li and SE meet[123–125] (Fig. 4a,b). The Li dendrite grows into the SEI or nucleates inside the solid electrolyte if the applied interphase overpotential (AIOP) at the Li side of the SEI is larger than the critical interphase overpotential (CIOP) of the SEI[23] (Fig. 4a–d). The CIOP value mainly depends on intrinsic properties of the SEI; specifically, a high lithiophobicity, a high ionic:electronic conductivity ratio[53] and a high mechanical strength lead to high CIOP values, which can effectively suppress Li dendrite nucleation and growth. This proposed Li dendrite growth mechanism can explain most results reported in the literature. For example, the high electronic conduction of solid electrolytes and SEIs causes the CIOP to decrease, thus promoting Li dendrite growth into solid electrolytes or even direct nucleation inside solid electrolytes[22,119,120], although it also causes the AIOP to decrease slightly. The void accumulation at the Li side of the SEI during Li plating–stripping cycles raises the interfacial resistance, thus increasing the AIOP and promoting Li dendrite growth[57,58,60]. Increasing Li diffusivity with Li–M (M = alloy metal) alloy anodes and increasing the Li creep rate by applying a high stack pressure increases the void-refilling rate and ameliorates the formation of voids at the Li side of the SEI[52,61,126], thus decreasing AIOP and suppressing lithium dendrite growth. The balanced ionic and electronic conductivity of interlayers can reduce the AIOP:CIOP value ratio, thus the electronic–ionic mixed conductive interlayers can suppress Li dendrite growth[127].

Even if Li nucleates and grows inside solid electrolytes, the CIOP can still be used to evaluate the Li dendrite suppression capability in the solid electrolyte. Li nucleation in solid electrolytes also leads to the formation of an SEI between nucleating Li and the solid electrolyte. The growth of nucleated Li inside solid electrolytes is similar to the Li deposition at the interface between Li and SEIs. Additionally, the property of the solid electrolyte indirectly affects the property of the SEI, in a situation in which high CIOPs and low AIOPs not only suppress Li dendrite growth, but also prevent Li nucleation inside solid electrolytes as the SEI ensures a potential larger than 0 V versus Li^+/Li at the surface of the solid electrolyte. If a solid electrolyte has high electronic conductivity, the formed SEI will also have high electronic conductivity, which will cause the CIOP to decrease. Therefore, the CIOP can be used to guide the design of solid electrolytes and SEIs.

Strategies for Li dendrite suppression. As discussed, lithium dendrite growth can be suppressed by reducing the value of the AIOP:CIOP ratio to less than 1; CIOP is the intrinsic resistance of the SEI for lithium dendrite growth and is affected by the lithiophobicity and mechanical strength of the SEI, and AIOP is the driving force of lithium dendrite growth, which is affected by the Li and solid electrolyte interfacial contact and the electronic and ionic conductivity of the SEI. A high electronic conductivity of the SEI can reduce the AIOP, but it also reduces the CIOP, as Li will prefer to plate at the interface between the solid electrolyte and the SEI, and continuously reduce the solid electrolyte forming an electronically conductive SEI, promoting Li dendrite growth. How to optimize the design of solid electrolytes, the interface

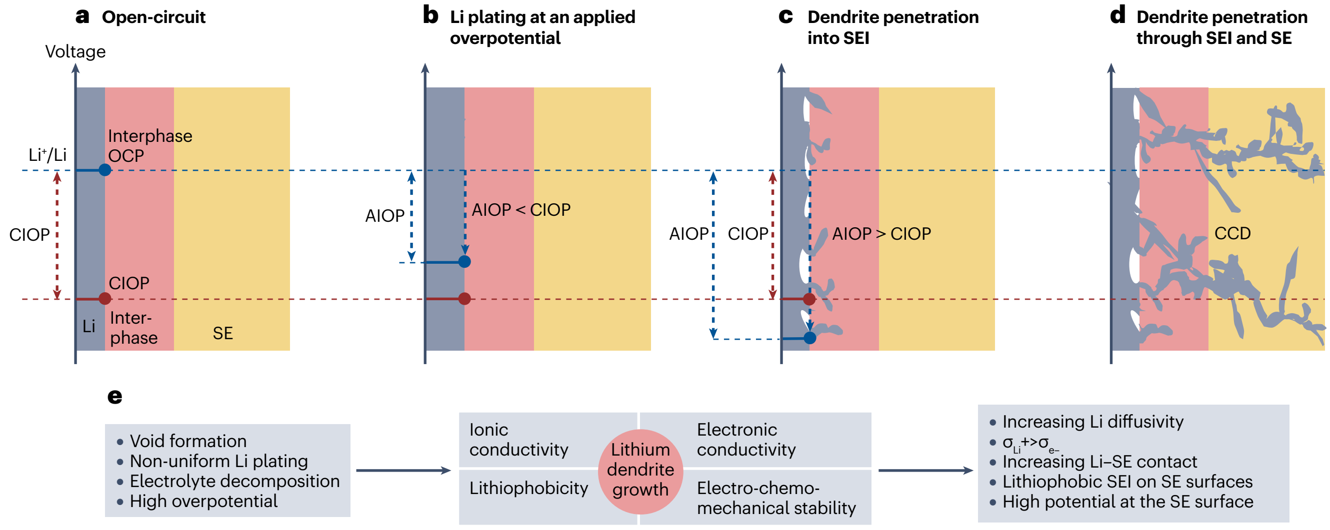

Fig. 4 | Li dendrite growth in an all-solid-state battery. Illustration of the correlation between critical interphase overpotential (CIOP), applied interphase overpotential (AIOP) and critical current density (CCD) at open-circuit (part **a**), when Li-plating at AIOP < CIOP (part **b**) and at AIOP > CIOP (part **c**), and when Li has penetrated through the solid electrolyte interphase (SEI) and the solid electrolyte (SE) (part **d**). **e**, Summary of the factors leading to lithium dendrite growth, the problems associated with this growth and the strategies for ameliorating it[56,143,144]. Left, problems that lead to lithium dendrite growth; middle part: factors that affect lithium dendrite growth; right, strategies that suppress lithium dendrite growth. OCP, open-circuit potential; σ_{e^-}, electronic conductivity; σ_{Li^+}, lithium ion conductivity. Adapted from ref. 23, Springer Nature Limited.

between Li and the SEI, as well as the SEI itself, to achieve a lithium dendrite-free all-solid-state battery with low interface resistance even at high Li plating capacity, is still unknown.

In the following paragraphs, we summarize the progress in Li and solid electrolyte interface design, as well as in SEI and solid electrolyte modifications, and we describe the challenges for designing high-capacity ASSLBs and how the illustrated design and modification strategies affect CIOP and AIOP. Finally, a promising interface design strategy for lithium dendrite-free anode is proposed to maximize the energy density of all-solid-state batteries.

Reducing the value of the interface resistance is an important consideration when attempting to decrease the AIOP. As discussed above, the AIOP:CIOP ratio has to be less than 1 to suppress lithium dendrite growth at the Li side of the SEI. To decrease AIOP, the value of the interfacial resistance at the interface between Li and SEI has to be reduced. One way to achieve this goal is to increase the Li and solid electrolyte interfacial contact area[57,128,129], which is affected by two key factors: first, the void formation and refilling rate, and second, Li wettability on the solid electrolyte and SEI. During Li stripping, voids will form at the Li–solid electrolyte interface, when the Li diffusion rate is lower than the Li stripping rate. If the voids formed during Li stripping are not refilled during the following Li plating process, voids will accumulate at Li and solid electrolyte interface, leading to lithium dendrite growth (Fig. 5A). As such, void formation is related to Li diffusivity. For example, the introduction of 10 atomic percentage Mg into a Li electrode can cause the effective Li diffusivity coefficient to increase from 0.8×10^{-11} cm^2 s^{-1} to 2.3×10^{-11} cm^2 s^{-1}, resulting in an increase in the Li stripping capacity from 0.9 mAh cm^{-2} for Li anodes to ~1.5 mAh cm^{-2} for Li–Mg alloy anodes, before contact-loss occurs at the Li and $Li_{6.25}Al_{0.25}La_3Zr_2O_{12}$ interface (the Li stripping current density was fixed at 0.1 mA cm^{-2})[61]. Void formation is also related to the temperature at which experiments are run. An increase of the testing temperature can increase Li creep rate and Li diffusivity[130], thus increasing the void refilling rate. Likewise, the stack pressure is an important factor. A high stack pressure can force Li to creep towards the SEI[131,132], preventing void formation during Li stripping, and an increase in overpotential during Li plating. Therefore, a high stack pressure should be applied for the ASSLB using two-dimensional Li anodes to achieve fast-charging performances. However, a high stack pressure is not desired for industrial applications. How to prevent void formation at low stack pressure is also a critical issue that needs to be addressed. Now, we focus on the second key point of increasing the wettability of Li on SEI and solid electrolyte. Introducing two-dimensional lithiophilic metal alloys (2D-M, where M = Au, Ag, Mg, Sb, Sn, Zn and other metals) on the solid electrolyte surface is beneficial for reducing Li and SEI (or solid electrolyte) interfacial resistance before cell cycles[133,134]. Constructing three-dimensional (3D) Li hosts or using a self-healable liquid alloy anode can ameliorate the interfacial contact loss at a lower stack pressure. By replacing the 2D-M layer with a 3D-M layer, the stress generated during planar Li plating at the 2D-M and SEI interface can be lessened due to the more uniform current distribution at the 3D-M and SEI interface. Furthermore, by replacing the solid alloy interlayer with a flowable liquid alloy, void formation during Li stripping and stress concentration at the boundary of the voids during Li plating can be substantially prevented at low stack pressure. For example, when using a Na–K liquid alloy at the Li and $Li_{6.75}La_3Zr_{1.75}Ta_{0.25}O_{12}$ interface (Fig. 5B), the Li||Li symmetric cell can even cycle at a capacity up to 3.5 mAh cm^{-2} at the relatively low stack pressure of 75 kPa[56]. Similarly, the use of liquid Ga at the Li and Li_2CO_3 interface in the Li/Li_2CO_3-$Li_{6.5}La_3Zr_{1.5}Ta_{0.5}O_{12}$-$Li_2CO_3$/Li cell[135] can also increase the affinity between Li and Li_2CO_3. Li–Ga alloy anodes are characterized by a higher Li diffusivity than pure Li metal anodes, so use of the former can further stabilize the Li and $Li_{6.5}La_3Zr_{1.5}Ta_{0.5}O_{12}$ interface. These strategies for improving the Li and solid electrolyte interfacial stability can reduce the AIOP at the interface of Li and the in situ-formed SEI due to the increased interfacial contact between Li and SEI during Li plating.

Also important to consider is the SEI design, in order to increase the CIOP. The intrinsic property (chemical, electrochemical and mechanical stability) of the SEI affects the CIOP value, in a context in which the electronic conductivity of the SEI and solid electrolyte will lead to lithium dendrite growth or even nucleation inside the solid electrolyte[22]. Decreasing the electronic conductivity of the solid electrolyte and increasing lithiophobicity of the in situ-formed SEI through fluorine[120,136] or iodine[124] doping leads to an increase in lithium dendrite suppression capability of the formed SEI layer as the CIOP increases. Since most solid electrolytes (such as $Li_7La_3Zr_2O_{12}$, Li_6PS_5Cl and Li_3PS_4)[52,58,121,122,137] are lithiophilic, Li dendrite penetration into these solid electrolytes form new SEIs with low CIOP. The volume change during Li penetration and SEI formation also leads to crack formation (Fig. 5C), which itself can lead to cell failure. For example, an Li_2S–Li_3P reduction layer (an SEI) can form at Li–Li_3PS_4 interfaces before Li plating and stripping cycles (Fig. 5Da,b). After Li plating, small cracks (marked by the blue lines) can form inside the SEI due to the volume expansion resulting from the decomposition reaction of the Li_3PS_4 layer (Fig. 5Dc), and Li is deposited along the cracks inside the SEI layer (marked by the pink area in the white circles; Fig. 5De). With further Li plating, new SEIs and cracks form inside the Li_3PS_4 layer (Fig. 5Df), followed by the formation of Li clusters in the cracks (Fig. 5Dg). The formation of Li clusters generates larger cracks; subsequently, Li penetration combined with the large cracks leads to cell failure (Fig. 5Dh,i) in solid electrolytes with poor stability towards Li. Introducing LiI into the Li_3PS_4 layer can prevent the formation of a reductive SEI after Li penetrates into the solid electrolyte (Fig. 5Dj) due to the formation of lithiophobic LiI-rich SEI at the Li and solid electrolyte interface, where no dark-contrast area forms near the lithium deposition area. By sharp contrast, the reduction layer along with the lithium clusters (marked by the white circles in Fig. 5Dh) forms in the Li_3PS_4 electrolyte. Increasing the fracture toughness of the solid electrolyte can also increase the lithium dendrite suppression capability; for example, applying a compressive force on $Li_{6.6}La_3Ta_{0.4}Zr_{1.6}O_{12}$ can reduce the probability of Li dendrite penetration perpendicular to the applied pressure[138]. In summary, the chemical, electrochemical and mechanical instabilities of solid electrolyte and Li interfaces lead to Li dendrite formation. Since the solid electrolyte is lithiophilic, the formation of SEI will generate strain, leading to crack formation. The formed cracks in the SEI and solid electrolyte promote Li penetration further into the cracks due to surface forces, resulting in Li dendrite growth along the cracks. Therefore, improving the electrochemical stability and fracture toughness of solid electrolytes and increasing the lithiophobicity of the SEI can suppress lithium dendrites[121,138].

Adding an artificial SEI at the Li–solid electrolyte interface can simultaneously increase CIOP and decrease AIOP. Even though improving the chemical, electrochemical and mechanical stability of solid electrolytes can reduce the probability of Li nucleation and dendrite growth, it can still not fully prevent dendrite growth, thus limiting the capacity for Li plating. To prevent dendrite growth into the solid electrolyte layer at a high Li plating capacity, an artificial SEI layer with a high CIOP has to be inserted at the Li–solid electrolyte interface. Generally, SEIs with high lithiophobicity, high mechanical strength and a high ionic:electronic conductivity ratio have high CIOPs. LiF SEIs are characterized by high lithiophobicity and high mechanical strength[139], but the low ionic conductivity and poor contact at the interface between Li and LiF increase the AIOP. The introduction of lithiophilic Mg at the interface between Li and LiF[140] can reduce the AIOP by increasing the interfacial contact between LiF and Li, thus supressing dendrite growth. Similarly, the Ag@C layer (a mixture of Ag nanoparticles and carbon black powder) that is artificially inserted at the Li–Li_6PS_5Cl interface can also effectively suppress lithium dendrite growth. After Li plating and

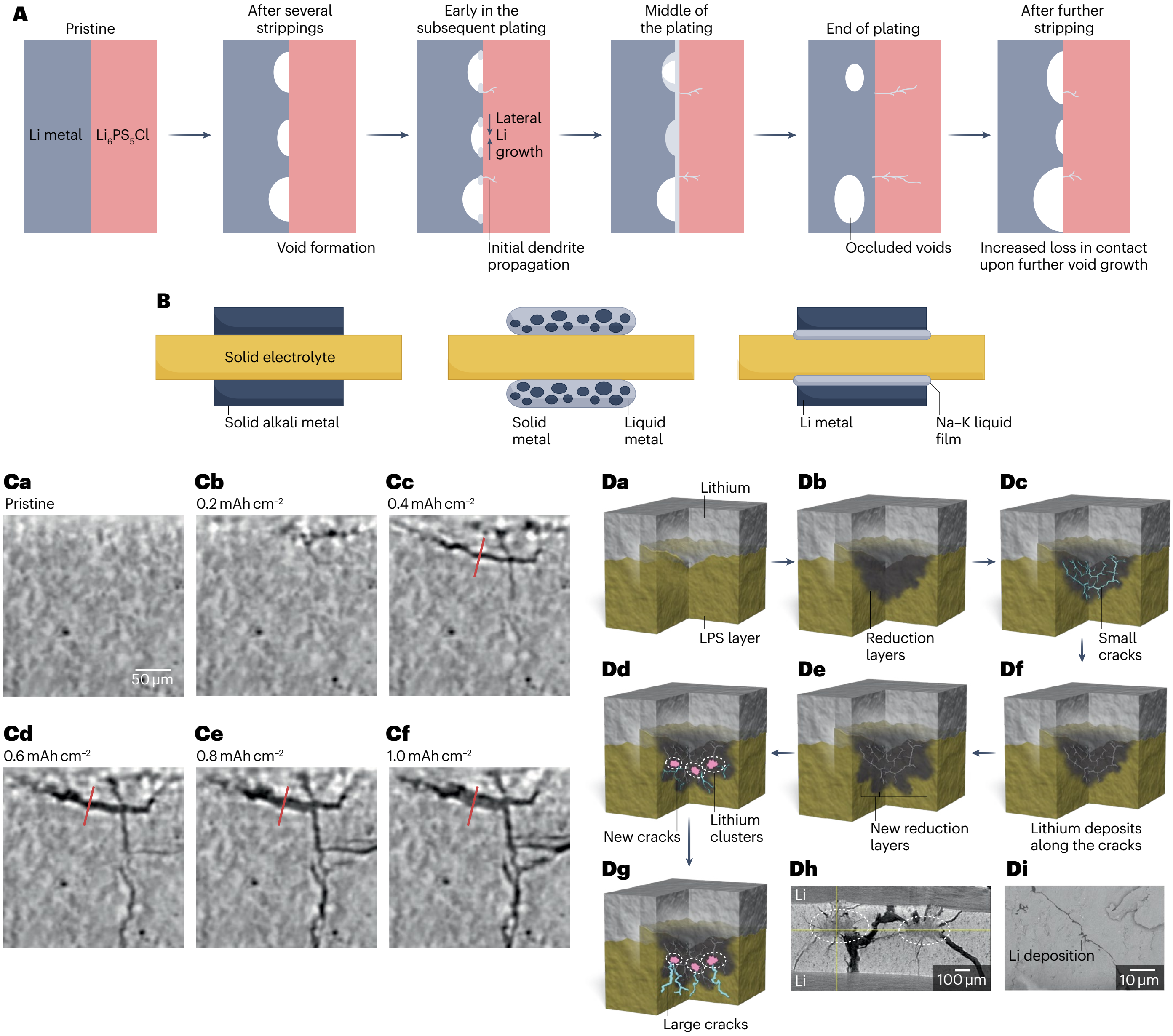

Fig. 5 | Cell failure (lithium dendrite growth and/or crack formation) mechanism and strategies to prevent dendrite growth and crack formation. **A**, Illustration of void formation at Li and Li_6PS_5Cl interface[57]. Voids form during Li plating and stripping cycles and promote lithium dendrite propagation into the Li_6PS_5Cl bulk as more Li is plated. At the end of plating, voids can be found in the Li metal, but further voids form upon repeated stripping, leading to greater contact loss between Li and Li_6PS_5Cl. **B**, Improving the Li–solid electrolyte contact and preventing stress concentration by using Na–K liquid metal. Changing the anode in a cell from pure, solid alkali metal (left) to semi-solid electrode (middle; the liquid metal is a Na–K alloy), to a liquid metal-buffered anode (right) can considerably improve the cell performance[56]. **C**, Lithium penetration and crack growth (as seen in black) in a Li_6PS_5Cl electrolyte after Li plating at increasing current densities (from 0.2, 0.4, 0.6, 0.8 to 1.0 mAh cm^{-2})[58]. **D**, Li plating in Li_3PS_4 (LPS; parts **Da**–**Dh**) and LiI-doped LPS electrolytes[137] (part **Di**). An illustration (part **Dg**) and tomogram (part **Dh**) of the Li/LPS/Li cell after short-circuiting is also shown. The pink area marked in white circles indicates lithium clusters, and the blue lines indicate the cracks. A back-scattered electron image (part **Di**) of a LPS-LiI pellet after short-circuiting showing cracks and Li depositions (in black) is also displayed. Part **a** adapted from ref. 57, Springer Nature Limited; part **b** adapted from ref. 56, Springer Nature Limited; part **c** adapted from ref. 58, Springer Nature Limited; part **d** adapted with permission from ref. 137, ACS.

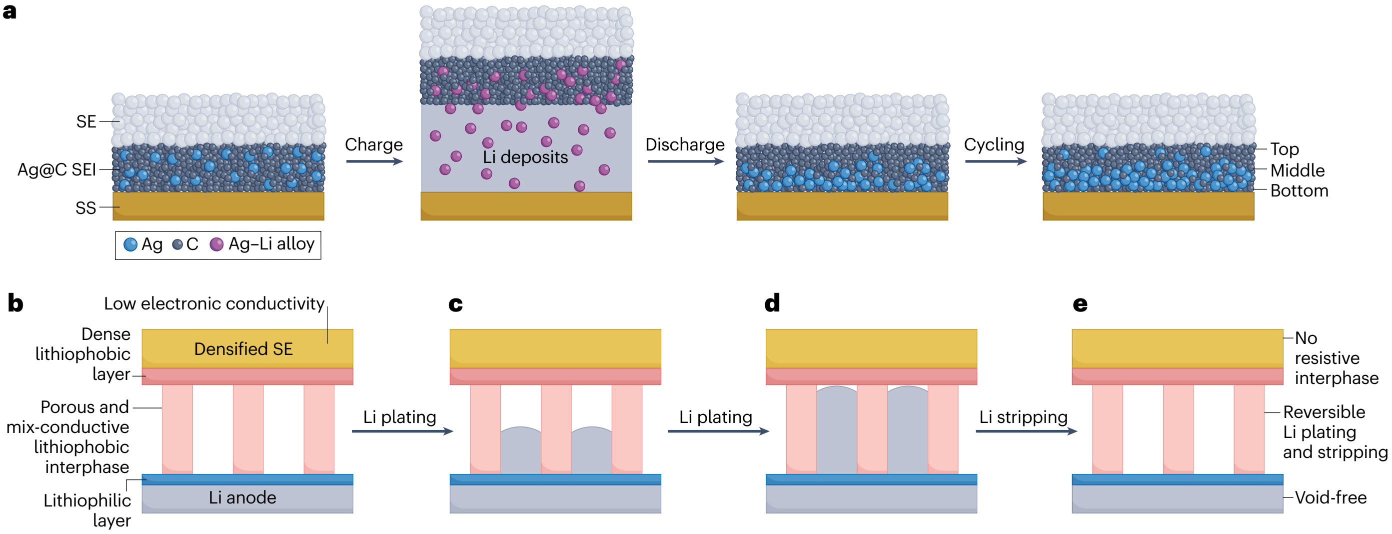

Fig. 6 | Interface design for lithium dendrite suppression. a, Illustration of the Li plating and stripping processes and the Ag@C solid electrolyte interphase (SEI) evolution in the Li_6PS_5Cl-Ag@C-Li structure[55], in which Li_6PS_5Cl is the solid electrolyte (SE), the Ag@C SEI is a mixture of Ag nanoparticles and carbon black powder. Li deposits at the interface between C and the stainless steel (SS) current collector during charging. After discharge, Li is fully stripped, whereafter the initial charge–discharge process, the Li_6PS_5Cl-Ag@C-Li structure changes to Li_6PS_5Cl-C-Ag due to the migration of Ag from Ag@C towards the SS during Li deposition. **b**, A proposed structure to achieve a high-capacity, fast-charging and lithium dendrite-free all-solid-state lithium battery, in which the SE layer should have high densification and low electronic conductivity; the top sub-layer on the surface of SE has to be lithiophobic; the bottom sub-layer on the surface of Li anode has to be lithiophilic; the middle sub-layer between the top lithiophobic layer and the bottom lithiophilic layer has to be porous, electronic–ionic mixed conductive and lithiophobic. **c**–**e**, Li plating (parts **c**,**d**) and stripping (part **e**) processes in the proposed structure. Part **a** adapted from ref. 55, Springer Nature Limited.

stripping cycles, the Li_6PS_5Cl-Ag@C-Li structure transforms into the Li_6PS_5Cl-C-LiAg structure due to the migration of Ag to the deposited Li[55] (Fig. 6a). The lithiophobic carbon in contact with Li_6PS_5Cl has a high CIOP, whereas LiAg with high Li diffusivity[141] decreases the AIOP, enabling a uniform Li deposition at Li–C interfaces, instead of at the Li_6PS_5Cl–C interface, thus preventing Li dendrite growth during Li plating. Changing the planar Li plating–stripping[139] behaviour at two-dimensional Li–SEI interfaces to a three-dimensional (3D) Li plating–stripping behaviour inside the porous and lithiophobic LiF–Li_3N composite SEI can considerably increase the critical current density of Li_3PS_4 electrolytes[142] due to the decrease of the AIOP. However, the main drawback of the porous and lithiophobic LiF–Li_3N layer is its limited Li-plating capacity, as once all the pores are filled with Li, the solid electrolyte will be reduced, and an SEI with a low CIOP forms on the solid electrolyte surface. To ensure a high Li-plating capacity at a low stack pressure, the 3D lithiophobic interlayer has to attain a AIOP:CIOP of less than 1 ref. 23, which can be achieved by a combination of the following four requirements (Fig. 6a–e): first, an intimate interfacial contact at the Li–SEI interface is necessary, and Li diffusivity inside the Li electrode should be high to prevent void formation during Li plating and stripping cycles — similar to the in situ construction of the LiAg and C interface after Ag migrated from the Ag@C[55] layer into the Li layer. Second, the SEI layer that is in contact with the solid electrolyte has to be lithiophobic or electronically insulating, similar to the in situ formation of lithiophobic C SEIs between LiAg and Li_6PS_5Cl. Third, the solid electrolyte layer should have low electronic conductivity, high densification and high fracture toughness, similar to the construction of the very dense Li_6PS_5Cl electrolyte made through warm isostatic pressing at 490 MPa. Fourth, to further relieve the stresses arising during Li plating at the Li–SEI interface, a 3D porous Li host should be introduced. The optimized Li–solid electrolyte interface should be composed of three parts (Fig. 6b–e), in a situation in which the top layer in contact with the solid electrolyte has to be lithiophobic to prevent the reduction of the solid electrolyte by the deposited Li; the middle lithiophobic layer has to be porous and electronic–ionic mixed conductive to ameliorate stress concentration during Li plating, enabling reversible Li plating and stripping inside the pores of this middle layer at high capacity; the bottom lithiophilic layer on the Li surface must ensure good contact between the Li anode and the interphase. Apart from the interphase, the solid electrolyte must have a high densification and low electronic conductivity to prevent Li nucleation inside the solid electrolyte. Using such optimized structures, lithium dendrite-free ASSLBs with high Li plating capacity at a low stack pressure can be created.

Summary and perspective

Electrolyte design is critical to the development of advanced batteries with superior performance. The bulk properties of the electrolytes are important, but so too is the interfacial chemistry that results in the formation of the SEI and CEI at the electrolyte–electrode interface, which influences the electrochemical performance. An unstable SEI promotes lithium dendrite growth and induces electrolyte depletion, whereas unstable CEIs accelerate the loss of the active material, which leads to a decay in its fast-charging capacity and, eventually, to cell short circuit. To clarify the impact of the SEI and CEI on the electrochemical performance of the cell, we first discussed the interfacial chemistries in individual aqueous electrolytes, non-aqueous electrolytes and solid electrolytes. The underlying interaction among these systems was then covered; lithiophobic LiF interphases can overcome the challenges at both the anode and cathode in different battery systems due to their wide ESW (0.0–6.5 V), high mechanical strength, high ionic:electronic conductivity ratio and weak bonding to electrode materials. These merits of LiF interfaces can ensure their high electrochemical-chemical-mechanical stability during cell cycling. The stable LiF interphase enables the successful application of high-voltage and high-capacity cathodes and anodes, which greatly improves the cell-level energy density compared with commercial Li-ion batteries. To guide the electrolyte-interphase design for next-generation batteries with high energy density and high safety, we suggest the electrolyte design to focus on the following objectives: i) electrolytes should be non-flammable to ensure safety; ii) both SEI and CEI should be weakly bonded to the electrode and have high mechanical strength to withstand the volume change of the electrode material, so as to prevent electrolyte depletion, thus increasing the cell cycle life; iii) the formed CEI should have a high oxidation stability to allow the use of high-voltage cathode materials and the generation of a fast ionic conduction pathway to enable fast-charging; iv) the formed SEI should have a high interface energy with the anode, as well as a low AIOP and high CIOP to suppress lithium dendrite growth — especially at high Li plating capacity. However, the answers to the fundamental questions of how to construct SEIs and CEIs with tuneable composition are not fully known. More interdisciplinary collaboration is needed to gain further insight into the SEI and CEI formation mechanisms to allow for greater optimization of batteries.

References

1. Xu, K. Electrolytes and interphases in Li-ion batteries and beyond. *Chem. Rev.* **114**, 11503–11618 (2014).
2. Rodrigues, M.-T. F. et al. A materials perspective on Li-ion batteries at extreme temperatures. *Nat. Energy* **2**, 17108 (2017).
3. Feng, X. et al. Thermal runaway mechanism of lithium ion battery for electric vehicles: a review. *Energy Storage Mater.* **10**, 246–267 (2018).
4. Xu, K. Nonaqueous liquid electrolytes for lithium-based rechargeable batteries. *Chem. Rev.* **104**, 4303–4418 (2004).
5. Kurzweil, P. Gaston Planté and his invention of the lead–acid battery — the genesis of the first practical rechargeable battery. *J. Power Sources* **195**, 4424–4434 (2010).
6. Li, W., Dahn, J. R. & Wainwright, D. S. Rechargeable lithium batteries with aqueous electrolytes. *Science* **264**, 1115–1118 (1994).
7. Suo, L. et al. "Water-in-salt" electrolyte enables high-voltage aqueous lithium-ion chemistries. *Science* **350**, 938–943 (2015).
8. Xu, J. et al. Aqueous electrolyte design for super-stable 2.5 V $LiMn_2O_4||Li_4Ti_5O_{12}$ pouch cells. *Nat. Energy* **7**, 186–193 (2022).
9. Fong, R., von Sacken, U. & Dahn, J. R. Studies of lithium intercalation into carbons using nonaqueous electrochemical cells. *J. Electrochem. Soc.* **137**, 2009–2013 (1990).
10. Pistoia, G., De Rossi, M. & Scrosati, B. Study of the behavior of ethylene carbonate as a nonaqueous battery solvent. *J. Electrochem. Soc.* **117**, 500–502 (1970).
11. Xu, K. Whether EC and PC differ in interphasial chemistry on graphitic anode and how. *J. Electrochem. Soc.* **156**, A751–A755 (2009).
12. Hobold, G. M. et al. Moving beyond 99.9% Coulombic efficiency for lithium anodes in liquid electrolytes. *Nat. Energy* **6**, 951–960 (2021).
13. Tan, J., Matz, J., Dong, P., Shen, J. & Ye, M. A growing appreciation for the role of LiF in the solid electrolyte interphase. *Adv. Energy Mater.* **11**, 2100046 (2021).
14. Zhang, Q. et al. *In situ* TEM visualization of LiF nanosheet formation on the cathode-electrolyte interphase (CEI) in liquid-electrolyte lithium-ion batteries. *Matter* **5**, 1235–1250 (2022).
15. Abe, T., Fukuda, H., Iriyama, Y. & Ogumi, Z. Solvated Li-ion transfer at interface between graphite and electrolyte. *J. Electrochem. Soc.* **151**, A1120–A1123 (2004).
16. Borodin, O. et al. Modeling insight into battery electrolyte electrochemical stability and interfacial structure. *Acc. Chem. Res.* **50**, 2886–2894 (2017).
17. Xu, J. et al. Electrolyte design for Li-ion batteries under extreme operating conditions. *Nature* **614**, 694–700 (2023).
18. Wang, Y. et al. Emerging electrolytes with fluorinated solvents for rechargeable lithium-based batteries. *Chem. Soc. Rev.* **52**, 2713–2763 (2023).
19. Jiao, S. et al. Stable cycling of high-voltage lithium metal batteries in ether electrolytes. *Nat. Energy* **3**, 739–746 (2018).
20. Manthiram, A., Yu, X. & Wang, S. Lithium battery chemistries enabled by solid-state electrolytes. *Nat. Rev. Mater.* **2**, 16103 (2017).
21. Wang, C. et al. Identifying soft breakdown in all-solid-state lithium battery. *Joule* **6**, 1770–1781 (2022).
22. Han, F. et al. High electronic conductivity as the origin of lithium dendrite formation within solid electrolytes. *Nat. Energy* **4**, 187–196 (2019).
23. Wan, H. et al. Critical interphase overpotential as a lithium dendrite-suppression criterion for all-solid-state lithium battery design. *Nat. Energy* **8**, 473–481 (2023).
24. Xu, K. Navigating the minefield of battery literature. *Commun. Mater.* **3**, 31 (2022).
25. Fong, K. D. et al. Ion transport and the true transference number in nonaqueous polyelectrolyte solutions for lithium ion batteries. *ACS Cent. Sci.* **5**, 1250–1260 (2019).
26. Zhang, J. et al. Interfacial design for a 4.6 V high-voltage single-crystalline $LiCoO_2$ cathode. *Adv. Mater.* **34**, e2108353 (2022).
27. Winter, M., Barnett, B. & Xu, K. Before Li ion batteries. *Chem. Rev.* **118**, 11433–11456 (2018).
28. Borodin, O. Challenges with prediction of battery electrolyte electrochemical stability window and guiding the electrode–electrolyte stabilization. *Curr. Opin. Electrochem.* **13**, 86–93 (2019).
29. Cheng, H. et al. Emerging era of electrolyte solvation structure and interfacial model in batteries. *ACS Energy Lett.* **7**, 490–513 (2022).
30. Zhang, Z. et al. Capturing the swelling of solid-electrolyte interphase in lithium metal batteries. *Science* **375**, 66–70 (2022).
31. Scharf, J. et al. Bridging nano- and microscale X-ray tomography for battery research by leveraging artificial intelligence. *Nat. Nanotechnol.* **17**, 446–459 (2022).
32. Xie, X. et al. Data-driven prediction of formation mechanisms of lithium ethylene monocarbonate with an automated reaction network. *J. Am. Chem. Soc.* **143**, 13245–13258 (2021).
33. Blau, S. M. et al. A chemically consistent graph architecture for massive reaction networks applied to solid-electrolyte interphase formation. *Chem. Sci.* **12**, 4931–4939 (2021).
34. Liu, J. et al. Pathways for practical high-energy long-cycling lithium metal batteries. *Nat. Energy* **4**, 180–186 (2019).
35. Stephan, A. K. Standardized battery reporting guidelines. *Joule* **5**, 1–2 (2021).
36. Schmuch, R., Wagner, R., Hörpel, G., Placke, T. & Winter, M. Performance and cost of materials for lithium-based rechargeable automotive batteries. *Nat. Energy* **3**, 267–278 (2018).
37. Waldmann, T., Wilka, M., Kasper, M., Fleischhammer, M. & Wohlfahrt-Mehrens, M. Temperature dependent ageing mechanisms in Lithium-ion batteries–a post-mortem study. *J. Power Sources* **262**, 129–135 (2014).
38. Nowak, S. & Winter, M. Chemical analysis for a better understanding of aging and degradation mechanisms of non-aqueous electrolytes for lithium ion batteries: method development, application and lessons learned. *J. Electrochem. Soc.* **162**, A2500–A2508 (2015).
39. Campion, C. L., Li, W. & Lucht, B. L. Thermal decomposition of $LiPF_6$-based electrolytes for lithium-ion batteries. *J. Electrochem. Soc.* **152**, A2327–A2334 (2005).
40. Chen, Y. et al. Engineering an insoluble cathode electrolyte interphase enabling high performance NCM811//graphite pouch cell at 60 °C. *Adv. Energy Mater.* **12**, 2201631 (2022).
41. Lin, D. et al. Fast galvanic lithium corrosion involving a Kirkendall-type mechanism. *Nat. Chem.* **11**, 382–389 (2019).
42. McBrayer, J. D. et al. Calendar aging of silicon-containing batteries. *Nat. Energy* **6**, 866–872 (2021).
43. Borodin, O., Self, J., Persson, K. A., Wang, C. & Xu, K. Uncharted waters: super-concentrated electrolytes. *Joule* **4**, 69–100 (2020).
44. Chen, L. et al. A 63 *m* superconcentrated aqueous electrolyte for high-energy Li-ion batteries. *ACS Energy Lett.* **5**, 968–974 (2020).
45. Yue, J. et al. Aqueous interphase formed by CO_2 brings electrolytes back to salt-in-water regime. *Nat. Chem.* **13**, 1061–1069 (2021).
46. Chen, J. et al. Improving electrochemical stability and low-temperature performance with water/acetonitrile hybrid electrolytes. *Adv. Energy Mater.* **10**, 1902654 (2020).
47. Wang, F. et al. Hybrid aqueous/non-aqueous electrolyte for safe and high-energy Li-ion batteries. *Joule* **2**, 927–937 (2018).
48. Shang, Y. et al. An "Ether-in-Water" electrolyte boosts stable interfacial chemistry for aqueous lithium-ion batteries. *Adv. Mater.* **32**, 2004017 (2020).
49. Giffin, G. A. The role of concentration in electrolyte solutions for non-aqueous lithium-based batteries. *Nat. Commun.* **13**, 5250 (2022).
50. Wang, J. et al. Superconcentrated electrolytes for a high-voltage lithium-ion battery. *Nat. Commun.* **7**, 12032 (2016).
51. Yao, Y. X. et al. Regulating interfacial chemistry in lithium-ion batteries by a weakly solvating electrolyte. *Angew. Chem. Int. Ed.* **60**, 4090–4097 (2021).
52. Dixit, M. B. et al. *In situ* investigation of chemomechanical effects in thiophosphate solid electrolytes. *Matter* **3**, 2138–2159 (2020).
53. Tu, Q., Shi, T., Chakravarthy, S. & Ceder, G. Understanding metal propagation in solid electrolytes due to mixed ionic-electronic conduction. *Matter* **4**, 3248–3268 (2021).
54. Fu, C. et al. Universal chemomechanical design rules for solid-ion conductors to prevent dendrite formation in lithium metal batteries. *Nat. Mater.* **19**, 758–766 (2020).
55. Lee, Y.-G. et al. High-energy long-cycling all-solid-state lithium metal batteries enabled by silver-carbon composite anodes. *Nat. Energy* **5**, 299–308 (2020).
56. Park, R. J. Y. et al. Semi-solid alkali metal electrodes enabling high critical current densities in solid electrolyte batteries. *Nat. Energy* **6**, 314–322 (2021).
57. Kasemchainan, J. et al. Critical stripping current leads to dendrite formation on plating in lithium anode solid electrolyte cells. *Nat. Mater.* **18**, 1105–1111 (2019).
58. Ning, Z. et al. Visualizing plating-induced cracking in lithium-anode solid-electrolyte cells. *Nat. Mater.* **20**, 1121–1129 (2021).
59. Chen, Y. et al. Li metal deposition and stripping in a solid-state battery via Coble creep. *Nature* **578**, 251–255 (2020).

60. Liu, X. et al. Local electronic structure variation resulting in Li ‘filament’ formation within solid electrolytes. *Nat. Mater.* **20**, 1485–1490 (2021).
61. Krauskopf, T., Mogwitz, B., Rosenbach, C., Zeier, W. G. & Janek, J. Diffusion limitation of lithium metal and Li–Mg alloy anodes on LLZO type solid electrolytes as a function of temperature and pressure. *Adv. Energy Mater.* **9**, 1902568 (2019).
62. Fan, X. et al. All-temperature batteries enabled by fluorinated electrolytes with non-polar solvents. *Nat. Energy* **4**, 882–890 (2019).
63. Michan, A. L., Leskes, M. & Grey, C. P. Voltage dependent solid electrolyte interphase formation in silicon electrodes: monitoring the formation of organic decomposition products. *Chem. Mater.* **28**, 385–398 (2016).
64. Shkrob, I. A., Wishart, J. F. & Abraham, D. P. What makes fluoroethylene carbonate different? *J. Phys. Chem. C* **119**, 14954–14964 (2015).
65. Shin, H., Park, J., Han, S., Sastry, A. M. & Lu, W. Component-/structure-dependent elasticity of solid electrolyte interphase layer in Li-ion batteries: experimental and computational studies. *J. Power Sources* **277**, 169–179 (2015).
66. Wang, C. et al. Self-healing chemistry enables the stable operation of silicon microparticle anodes for high-energy lithium-ion batteries. *Nat. Chem.* **5**, 1042–1048 (2013).
67. Choi, S., Kwon, T.-w, Coskun, A. & Choi, J. W. Highly elastic binders integrating polyrotaxanes for silicon microparticle anodes in lithium ion batteries. *Science* **357**, 279–283 (2017).
68. Li, Y. et al. Growth of conformal graphene cages on micrometre-sized silicon particles as stable battery anodes. *Nat. Energy* **1**, 15029 (2016).
69. Chen, J. et al. Electrolyte design for LiF-rich solid–electrolyte interfaces to enable high-performance microsized alloy anodes for batteries. *Nat. Energy* **5**, 386–397 (2020).
70. Yu, Z. et al. Molecular design for electrolyte solvents enabling energy-dense and long-cycling lithium metal batteries. *Nat. Energy* **5**, 526–533 (2020).
71. Yu, Z. et al. Rational solvent molecule tuning for high-performance lithium metal battery electrolytes. *Nat. Energy* **7**, 94–106 (2022).
72. Xue, W. et al. FSI-inspired solvent and “full fluorosulfonyl” electrolyte for 4 V class lithium-metal batteries. *Energy Environ. Sci.* **13**, 212–220 (2020).
73. Fan, X. et al. Non-flammable electrolyte enables Li-metal batteries with aggressive cathode chemistries. *Nat. Nanotechnol.* **13**, 715–722 (2018).
74. Liu, S. et al. An inorganic-rich solid electrolyte interphase for advanced lithium-metal batteries in carbonate electrolytes. *Angew. Chem. Int. Ed.* **60**, 3661–3671 (2021).
75. Chen, J. et al. Electrolyte design for Li metal-free Li batteries. *Mater. Today* **39**, 118–126 (2020).
76. Cao, X. et al. Monolithic solid–electrolyte interphases formed in fluorinated orthoformate-based electrolytes minimize Li depletion and pulverization. *Nat. Energy* **4**, 796–805 (2019).
77. Wang, Z. et al. An anion-tuned solid electrolyte interphase with fast ion transfer kinetics for stable lithium anodes. *Adv. Energy Mater.* **10**, 1903843 (2020).
78. Li, T. et al. Stable anion-derived solid electrolyte interphase in lithium metal batteries. *Angew. Chem. Int. Ed.* **60**, 22865–22869 (2021).
79. Suo, L. et al. Fluorine-donating electrolytes enable highly reversible 5-V-class Li metal batteries. *Proc. Natl Acad. Sci. USA* **115**, 1156–1161 (2018).
80. Chen, S. et al. High-voltage lithium-metal batteries enabled by localized high-concentration electrolytes. *Adv. Mater.* **30**, e1706102 (2018).
81. Phan, A. L. et al. Solvent-free electrolyte for high-temperature rechargeable lithium metal batteries. *Adv. Funct. Mater.* **33**, 2301177 (2023).
82. Ikeya, M. Electrical properties of lithium hydride. *J. Phys. Soc. Jpn.* **42**, 168–174 (1977).
83. Pan, J., Cheng, Y.-T. & Qi, Y. General method to predict voltage-dependent ionic conduction in a solid electrolyte coating on electrodes. *Phys. Rev. B* **91**, 134116 (2015).
84. Aurbach, D. & Weissman, I. On the possibility of LiH formation on Li surfaces in wet electrolyte solutions. *Electrochem. Commun.* **1**, 324–331 (1999).
85. Fang, C. et al. Quantifying inactive lithium in lithium metal batteries. *Nature* **572**, 511–515 (2019).
86. Zachman, M. J., Tu, Z., Choudhury, S., Archer, L. A. & Kourkoutis, L. F. Cryo-STEM mapping of solid–liquid interfaces and dendrites in lithium-metal batteries. *Nature* **560**, 345–349 (2018).
87. Shadike, Z. et al. Identification of LiH and nanocrystalline LiF in the solid–electrolyte interphase of lithium metal anodes. *Nat. Nanotechnol.* **16**, 549–554 (2021).
88. Xiang, Y. et al. Quantitatively analyzing the failure processes of rechargeable Li metal batteries. *Sci. Adv.* **7**, eabj3423 (2021).
89. Xu, G. et al. The formation/decomposition equilibrium of LiH and its contribution on anode failure in practical lithium metal batteries. *Angew. Chem. Int. Ed.* **133**, 7849–7855 (2021).
90. Zhang, H., Ju, S., Xia, G. & Yu, X. Identifying the positive role of lithium hydride in stabilizing Li metal anodes. *Sci. Adv.* **8**, eabl8245 (2022).
91. Huang, L. et al. Uncovering LiH triggered thermal runaway mechanism of a high-energy LiNi$_{0.5}$Co$_{0.2}$Mn$_{0.3}$O$_2$/graphite pouch cell. *Adv. Sci.* **8**, 2100676 (2021).
92. Gauthier, M. et al. Electrode–electrolyte interface in Li-ion batteries: current understanding and new insights. *J. Phys. Chem. Lett.* **6**, 4653–4672 (2015).
93. Jia, H. & Xu, W. Electrolytes for high-voltage lithium batteries. *Trends Chem.* **4**, 627–642 (2022).
94. Xu, J. Critical review on cathode–electrolyte interphase toward high-voltage cathodes for Li-ion batteries. *Nano-Micro Lett.* **14**, 166 (2022).
95. Tebbe, J. L., Fuerst, T. F. & Musgrave, C. B. Degradation of ethylene carbonate electrolytes of lithium ion batteries via ring opening activated by LiCoO$_2$ cathode surfaces and electrolyte species. *ACS Appl. Mater. Interfaces* **8**, 26664–26674 (2016).
96. Cárdenas, C. et al. Chemical reactivity descriptors for ambiphilic reagents: dual descriptor, local hypersoftness, and electrostatic potential. *J. Phys. Chem. A* **113**, 8660–8667 (2009).
97. Dose, W. M. et al. Onset potential for electrolyte oxidation and Ni-rich cathode degradation in lithium-ion batteries. *ACS Energy Lett.* **7**, 3524–3530 (2022).
98. Chen, Y.-Q. et al. An electrolyte additive with boron-nitrogen-oxygen alkyl group enabled stable cycling for high voltage LiNi$_{0.5}$Mn$_{1.5}$O$_4$ cathode in lithium-ion battery. *J. Power Sources* **477**, 228473 (2020).
99. Deng, T. et al. Designing in-situ-formed interphases enables highly reversible cobalt-free LiNiO$_2$ cathode for Li-ion and Li-metal batteries. *Joule* **3**, 2550–2564 (2019).
100. Chen, R. et al. An investigation of functionalized electrolyte using succinonitrile additive for high voltage lithium-ion batteries. *J. Power Sources* **306**, 70–77 (2016).
101. Pham, H. Q., Lee, H.-Y., Hwang, E.-H., Kwon, Y.-G. & Song, S.-W. Non-flammable organic liquid electrolyte for high-safety and high-energy density Li-ion batteries. *J. Power Sources* **404**, 13–19 (2018).
102. Wang, C. et al. Lithium difluorophosphate as a promising electrolyte lithium additive for high-voltage lithium-ion batteries. *ACS Appl. Energy Mater.* **1**, 2647–2656 (2018).
103. von Aspern, N. et al. Phosphorus additives for improving high voltage stability and safety of lithium ion batteries. *J. Fluor. Chem.* **198**, 24–33 (2017).
104. Wu, S. et al. Stabilizing LiCoO$_2$/graphite at high voltages with an electrolyte additive. *ACS Appl. Mater. Interfaces* **11**, 17940–17951 (2019).
105. Klein, S. et al. Re-evaluating common electrolyte additives for high-voltage lithium ion batteries. *Cell Rep. Phys. Sci.* **2**, 100521 (2021).
106. Tan, S. et al. Additive engineering for robust interphases to stabilize high-Ni layered structures at ultra-high voltage of 4.8 V. *Nat. Energy* **7**, 484–494 (2022).
107. Cherkashinin, G. et al. The stability of the SEI layer, surface composition and the oxidation state of transition metals at the electrolyte–cathode interface impacted by the electrochemical cycling: x-ray photoelectron spectroscopy investigation. *Phys. Chem. Chem. Phys.* **14**, 12321–12331 (2012).
108. Fan, X. & Wang, C. High-voltage liquid electrolytes for Li batteries: progress and perspectives. *Chem. Soc. Rev.* **50**, 10486–10566 (2021).
109. Xue, W. et al. Stabilizing electrode–electrolyte interfaces to realize high-voltage Li||LiCoO$_2$ batteries by a sulfonamide-based electrolyte. *Energy Environ. Sci.* **14**, 6030–6040 (2021).
110. Zheng, Q. et al. A cyclic phosphate-based battery electrolyte for high voltage and safe operation. *Nat. Energy* **5**, 291–298 (2020).
111. Xue, W. et al. Ultra-high-voltage Ni-rich layered cathodes in practical Li metal batteries enabled by a sulfonamide-based electrolyte. *Nat. Energy* **6**, 495–505 (2021).
112. Zhang, X. et al. Electrolyte regulating toward stabilization of cobalt-free ultrahigh-nickel layered oxide cathode in lithium-ion batteries. *ACS Energy Lett.* **6**, 1324–1332 (2021).
113. Ren, X. et al. Designing advanced in situ electrode/electrolyte interphases for wide temperature operation of 4.5 V Li||LiCoO$_2$ batteries. *Adv. Mater.* **32**, e2004898 (2020).
114. Liu, W. et al. Inhibition of transition metals dissolution in cobalt-free cathode with ultrathin robust interphase in concentrated electrolyte. *Nat. Commun.* **11**, 3629 (2020).
115. Xu, J. et al. Lithium halide cathodes for Li metal batteries. *Joule* **7**, 83–94 (2023).
116. Alvarado, J. et al. Bisalt ether electrolytes: a pathway towards lithium metal batteries with Ni-rich cathodes. *Energy Environ. Sci.* **12**, 780–794 (2019).
117. Mao, M. et al. In-situ construction of hierarchical cathode electrolyte interphase for high performance LiNi$_{0.8}$Co$_{0.1}$Mn$_{0.1}$O$_2$/Li metal battery. *Nano Energy* **78**, 105282 (2020).
118. Bai, P. et al. Formation of LiF-rich cathode-electrolyte interphase by electrolyte reduction. *Angew. Chem. Int. Ed.* **61**, e202202731 (2022).
119. Tian, H.-K., Xu, B. & Qi, Y. Computational study of lithium nucleation tendency in Li$_7$La$_3$Zr$_2$O$_{12}$ (LLZO) and rational design of interlayer materials to prevent lithium dendrites. *J. Power Sources* **392**, 79–86 (2018).
120. Mo, F. et al. Inside or outside: origin of lithium dendrite formation of all solid-state electrolytes. *Adv. Energy Mater.* **9**, 1902123 (2019).
121. Porz, L. et al. Mechanism of lithium metal penetration through inorganic solid electrolytes. *Adv. Energy Mater.* **7**, 1701003 (2017).
122. Zhang, L. et al. Lithium whisker growth and stress generation in an in situ atomic force microscope–environmental transmission electron microscope set-up. *Nat. Nanotechnol.* **15**, 94–98 (2020).
123. Narayanan, S. et al. Effect of current density on the solid electrolyte interphase formation at the lithium|Li$_6$PS$_5$Cl interface. *Nat. Commun.* **13**, 7237 (2022).
124. Han, F., Yue, J., Zhu, X. & Wang, C. Suppressing Li dendrite formation in Li$_2$S-P$_2$S$_5$ solid electrolyte by LiI incorporation. *Adv. Energy Mater.* **8**, 1703644 (2018).
125. Otto, S. K. et al. In situ investigation of lithium metal–solid electrolyte anode interfaces with ToF-SIMS. *Adv. Mater. Interfaces* **9**, 2102387 (2022).
126. LePage, W. S. et al. Lithium mechanics: roles of strain rate and temperature and implications for lithium metal batteries. *J. Electrochem. Soc.* **166**, A89–A97 (2019).
127. Kim, S. Y. & Li, J. Porous mixed ionic electronic conductor interlayers for solid-state batteries. *Energy Mater. Adv.* **2021**, 1519569 (2021).

128. Jow, T. R. & Liang, C. C. Interface between solid electrode and solid electrolyte — a study of the Li/LiI (Al_2O_3) solid-electrolyte system. *J. Electrochem. Soc.* **130**, 737–740 (1983).
129. Lu, Y. et al. The void formation behaviors in working solid-state Li metal batteries. *Sci. Adv.* **8**, eadd0510 (2022).
130. Bay, M. C. et al. Sodium plating from Na-β′′-Alumina ceramics at room temperature, paving the way for fast-charging all-solid-state batteries. *Adv. Energy Mater.* **10**, 1902899 (2020).
131. Wang, M. J., Choudhury, R. & Sakamoto, J. Characterizing the Li-solid-electrolyte interface dynamics as a function of stack pressure and current density. *Joule* **3**, 2165–2178 (2019).
132. Yan, H. et al. How does the creep stress regulate void formation at the lithium-solid electrolyte interface during stripping? *Adv. Energy Mater.* **12**, 2102283 (2022).
133. Choi, H. J. et al. In situ formed Ag-Li intermetallic layer for stable cycling of all-solid-state lithium batteries. *Adv. Sci.* **9**, 2103826 (2022).
134. Zhong, Y. et al. A highly efficient all-solid-state lithium/electrolyte interface induced by an energetic reaction. *Angew. Chem. Int. Ed.* **59**, 14003–14008 (2020).
135. Meng, J., Zhang, Y., Zhou, X., Lei, M. & Li, C. Li_2CO_3-affiliative mechanism for air-accessible interface engineering of garnet electrolyte via facile liquid metal painting. *Nat. Commun.* **11**, 3716 (2020).
136. Zhao, F. et al. Ultrastable anode interface achieved by fluorinating electrolytes for all-solid-state Li metal batteries. *ACS Energy Lett.* **5**, 1035–1043 (2020).
137. Otoyama, M. et al. Visualization and control of chemically induced crack formation in all-solid-state lithium-metal batteries with sulfide electrolyte. *ACS Appl. Mater. Interfaces* **13**, 5000–5007 (2021).
138. McConohy, G. et al. Mechanical regulation of lithium intrusion probability in garnet solid electrolytes. *Nat. Energy* **8**, 241–250 (2023).
139. Fan, X. et al. Fluorinated solid electrolyte interphase enables highly reversible solid-state Li metal battery. *Sci. Adv.* **4**, eaau9245 (2018).
140. Wan, H. et al. Bifunctional interphase-enabled $Li_{10}GeP_2S_{12}$ electrolytes for lithium–sulfur battery. *ACS Energy Lett.* **6**, 862–868 (2021).
141. Jin, S. et al. Solid-solution-based metal alloy phase for highly reversible lithium metal anode. *J. Am. Chem. Soc.* **142**, 8818–8826 (2020).
142. Ji, X. et al. Solid-state electrolyte design for lithium dendrite suppression. *Adv. Mater.* **32**, e2002741 (2020).
143. Yuan, C., Lu, W. & Xu, J. Unlocking the electrochemical–mechanical coupling behaviors of dendrite growth and crack propagation in all-solid-state batteries. *Adv. Energy Mater.* **11**, 2101807 (2021).
144. Kinzer, B. et al. Operando analysis of the molten Li|LLZO interface: understanding how the physical properties of Li affect the critical current density. *Matter* **4**, 1947–1961 (2021).

Acknowledgements

The authors acknowledge funding from the US Department of Energy (DOE) under Award number DEEE0008856, ARPA-E under Award of DE-AR0000781, Advanced Battery Materials Research (BMR) Program (Battery500 Consortium Phase 2) under DOE contract no. DE-AC05-76RL01830 from the Pacific Northwest National Laboratory (PNNL) and the US Department of Energy (DOE) through ARPA-E grant DEAR0000389.

Author contributions

H. W., J. X. and C. W. conceived the idea and wrote the draft. All the authors edited and revised the manuscript.

Competing interests

The authors declare no competing interests.

Additional information

Peer review information *Nature Reviews Chemistry* thanks the anonymous reviewers for their contribution to the peer review of this work.